

State-Estimator-Integrated Robust Adaptive Tracking Control for Flexible Air-breathing Hypersonic Vehicle with Noisy Measurements

Xinlong Tao, Jianqiang Yi, *Senior Member, IEEE*, Zhiqiang Pu, and Tianyi Xiong

This work was supported by NNSFC No. 61421004, 61603383, 61603384, and Beijing Advanced Innovation Center of Intelligent Robots and Systems under Grant 2016IRS23.

Xinlong Tao, Jianqiang Yi, Zhiqiang Pu, and Tianyi Xiong are with Institute of Automation, Chinese Academy of Sciences, Beijing, 100190 China, and with University of Chinese Academy of Sciences, Beijing, 100049 China (e-mail: {taoxinlong2014, jianqiang.yi, zhiqiang.pu, xiongtianyi2016}@ia.ac.cn).

Abstract—In this study, a novel state-estimator-integrated robust adaptive tracking control law is proposed for flexible air-breathing hypersonic vehicle (FAHV), with consideration of noisy measurements, parametric uncertainties, and unknown flexible dynamics. First, to reconstruct the states contaminated by the measurement noises, a continuous-model-based state estimator is designed, which can avoid severe phase lag problem brought by low-pass filter (LPF) and greatly improve the estimation accuracy in the transition process. Then, based on noise-free measurements, an ideal state feedback robust adaptive tracking controller is formulated to deal with the parametric uncertainties as well as unknown flexible dynamics, where interval type-2 fuzzy logic systems (IT2-FLSs) are employed to approximate the unknown dynamics of FAHV online. Lyapunov theorem is utilized to analyze the stability properties of the state estimator and the ideal state feedback tracking controller. By synthesizing the above two parts, the whole state-estimator-integrated robust adaptive tracking control law is finally developed. Comparative numerical simulations of four scenarios demonstrate the effectiveness and superiority of the proposed integrated control law.

Index Terms—hypersonic vehicle, measurement noises, robust control, state estimator, type-2 fuzzy logic system

I. INTRODUCTION

AIR-Breathing hypersonic vehicle (AHV), which can reach a speed over five Mach, has raised numerous attention all over the world for more than 60 years [1]. Since it is a promising way of accessing to space as well as prompt global strike, AHV technology reveals tremendous values in both military and commercial applications [2]. Recent successful flight tests include X-43A brought out by NASA and X-51A by US Air Force [3]. Owing to the complicated configuration of the vehicle as well as large flight envelope where atmospheric conditions significantly vary, AHV will suffer severe parametric uncertainties, which may directly affect the flight safety. Besides, the couplings between the scramjet engine and airframe will generate unknown structural flexibilities, which pose higher requirements on controller's robustness and thus should not be neglected in the design stage [4]. All of these features make the flight control design of flexible air-breathing hypersonic vehicle (FAHV) a real challenging work.

Facing the above challenges, numerous efforts have been made and great progress has been witnessed. In 2007, a nonlinear form of longitudinal truth model for FAHV was proposed by Bolender and Doman, which was widely employed in the subsequent investigations [5]. Based on this nonlinear longitudinal model, three typical control frameworks, including small-perturbation-based control [4], [6], input-output-linearization-based control [53], and back-stepping-based control [10], were further investigated. Among these three control frameworks, input-output-linearization-based control and back-stepping-based control became more and more appreciated due to the advantages of dealing with system nonlinearities. Recently, various advanced nonlinear control techniques, such as sliding mode control, adaptive control, fuzzy logic system, neural network, and their combinations, have been integrated into the above control frameworks to improve the flight performance [7]-[22]. In [9], a quasi-continuous high-order sliding mode controller together with a high order sliding mode observer was proposed to realize robust tracking performances of velocity and altitude against different fuel levels. Based on Lyapunov stability analysis, Fiorentini et al. developed a nonlinear robust adaptive controller for FAHV [10]. Considering parametric uncertainties and fuel level changes, Gao et al. proposed a novel indirect adaptive interval type-2 fuzzy sliding mode controller to keep all the signals in close-loop system bounded [14]. In [16], wind effects were taken into consideration, while a disturbance observer based adaptive controller was formulated using neural approximation. Bu et al. constructed two low-pass filters based on model transformations to handle non-affine problems, and proposed a novel improved neural back-stepping control strategy for FAHV [19]. With consideration of non-minimum phase behavior of FAHV longitudinal dynamics, Ye et al. established an output-redefinition-based dynamic inversion controller, in which output redefinition was used to make modified zero dynamics stable [20]. Besides, Hu et al. developed a robust adaptive fuzzy tracking controller to simultaneously deal with parametric uncertainties and unmodeled

dynamics [21]. Moreover, considering the difficulties in measuring flight path angle and angle of attack in practice, several output feedback control strategies were brought out, where in the first step the unmeasurable states were reconstructed through specific designed observers and then fed into the controller, as done in [23]-[27].

Nevertheless, in the existing literature, most results for FAHV assume that noise-free measurements are available for control design, which is actually impractical in real engineering. Due to high speed operation as well as extreme flight environment, mechanical and electromagnetic vibrations inevitably exist, which can generate considerable measurement noises in both pneumatic height sensor's and Mach sensor's outputs [28]-[30]. Directly utilizing these noise-contaminated signals for FAHV tracking control can result in extra high-frequency control actions, which means more actuator abrasions and energy wastes, performance degradation, and even flight failure. Although some verification simulations of system stability in presence of measurement noises are conducted in recent investigations [23], [26], and [31], seldom of them specifically consider the effects of measurement noises on FAHV responses in the control design stage, which motivates this study.

Generally, there are four common ways for control applications to cope with measurement noises in literature. The first one is low-pass filter (LPF), which is the most popular method in real engineering. Usually LPF is employed in cascade with a controller to filter out high-frequency components of the noises [32]-[34]. However, severe phase lag phenomenon will be brought by LPF, which is not considered in the design stage. For tracking problems where reference signals are not static, this phenomenon will lead to large tracking error in the transition process, which we do not expect for. The second is Kalman filter, including linear Kalman filter, extended Kalman filter (EKF) [35], and unscented Kalman filter (UKF) [36]. For nonlinear estimation issues, UKF, which can deal with the nonlinearity approximation problems of EKF through a probabilistic approach, shows a higher order of accuracy in state estimation and is easier for implementation in practice [37]. Various Kalman filters have been proposed and applied in different occasions, such as motion tracking, orientation estimation, and so on [38]-[42]. Nevertheless, Kalman filter is highly sensitive to modeling errors, such as unmodeled dynamics, parametric uncertainties, external disturbances, and so on. For those highly nonlinear and uncertain systems, such as FAHV, it is very difficult to obtain the whole precise model information, thus a serious deterioration of Kalman filtering performance may occur. The third way is the desired compensation adaptive control strategy, as introduced in [43]-[45]. This strategy aims to construct an additional noise-free adaptive model-based feed-forward control law such that the feedback gains in the controller can be correspondingly chosen small, which can alleviate the effects of measurement noises on system responses to some extent. In fact, the robustness of this control strategy depends on enough compensation brought by the adaptive feed-forward control law. Thus, learning ability of the designed adaptive system must be guaranteed, which requires extensive experiments and tests. Besides, high-frequency noises cannot be filtered out with this strategy, which acts as another drawback. The last one is called state-estimator-based control design, which was recently investigated in [46] and [47]. Since the state estimator can reconstruct the exact states from noisy measurements, it seems to be a promising way for noise suppression. Following this idea, Tao et al. proposed an adaptive interval type-2 fuzzy logic control scheme for FAHV, where state estimator is employed to restrain the noises of velocity and altitude measurements [48]. However, the effects of parametric uncertainties are not evaluated in their simulations. Furthermore, this control scheme is constructed based on a dynamic inversion controller, with which strong robustness are hard to obtain.

Based on the above observations, we propose a novel state-estimator-integrated robust adaptive tracking control law for FAHV in this study. Different from the issues in [23]-[27], additive measurement noises in the velocity channel and altitude channel are taken into consideration, thus for the velocity and altitude states, only noise-contaminated states can be utilized for control design, while other rigid-body states are assumed to be available and noise-free. First, a continuous-model-based state estimator is designed to estimate the exact states of velocity and altitude. Especially, the superiority of the state estimator over first-order LPF is stressed on. Then, an ideal state feedback robust adaptive tracking controller is formulated to deal with the parametric

uncertainties and unknown flexible dynamics based on noise-free measurements, where interval type-2 fuzzy logic systems (IT2-FLSs) are adopted to approximate the unknown dynamics of FAHV online. By synthesizing the state estimator and the ideal state feedback tracking controller, the whole state-estimator-integrated robust adaptive tracking control law is finally developed. Extensive numerical simulations are conducted to verify the effectiveness and superiority of our proposed integrated control law. The highlights of this study can be organized as follows. First, different from the most existing robust control designs for FAHV, which only consider the parametric uncertainties and model disturbances, the proposed integrated control law specifically deals with the measurement noises in the velocity channel and altitude channel, and the effectiveness is demonstrated through extensive simulation results. Second, compared with first-order LPF, the proposed state estimator can greatly improve the estimation accuracy in the transition process. Besides, it also shows a stronger robustness property against modeling errors than UKF so that a better tracking performance can be realized. Last, since the state estimator is a continuous-model-based one, Lyapunov theorem can be directly utilized for stability analysis. Moreover, the state estimator can be easily integrated into the robust adaptive tracking controller, which is appreciated for implementations in real engineering.

The rest of the paper is organized as follows. Section II briefly states the FAHV longitudinal model and formulates the main problem. In Section III, the proposed state-estimator-integrated robust adaptive tracking control design is described in detail. Comparative simulation results are presented and discussed in Section IV. Finally, we draw our conclusion in Section V.

II. PROBLEM FORMULATION

A. FAHV Longitudinal Model

This study mainly investigates the tracking control design for FAHV in cruise flight stage, where the longitudinal motion problem becomes the main issue. The geometry of FAHV longitudinal model is depicted in Fig. 1. With the achievements obtained by Bolender and Doman, the FAHV longitudinal dynamics adopted in this study can be described by the following differential equations [10]:

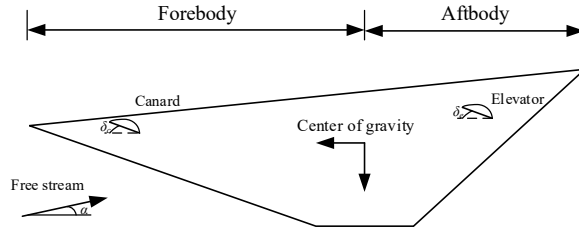


Fig. 1 Geometry of FAHV longitudinal model.

$$\dot{V} = (T \cos \alpha - D) / m - g \sin \gamma \quad (1)$$

$$\dot{h} = V \sin \gamma \quad (2)$$

$$\dot{\gamma} = (L + T \sin \alpha) / (mV) - g \cos \gamma / V \quad (3)$$

$$\dot{\alpha} = q - \dot{\gamma} \quad (4)$$

$$\dot{q} = M_{yy} / I_{yy} \quad (5)$$

$$\ddot{\eta}_i = -2\zeta_i \omega_i \dot{\eta}_i - \omega_i^2 \eta_i + N_i, \quad i = 1, 2, 3. \quad (6)$$

This model is comprised of five rigid-body states $\mathbf{x}_r = [V \ h \ \gamma \ \alpha \ q]^T$ and six flexible states $\boldsymbol{\eta} = [\eta_1 \ \dot{\eta}_1 \ \eta_2 \ \dot{\eta}_2 \ \eta_3 \ \dot{\eta}_3]^T$ corresponding to the first three bending modes of the fuselage, where V is the velocity, h is the altitude, γ is the flight path angle, α is the angle

of attack, while q is the pitch rate. Besides, m , g , I_{yy} , ζ_i , and ω_i are the mass, acceleration of gravity, moment of inertia, damping ratio, and flexible-mode frequency, respectively. The lift L , drag D , thrust T , pitching moment M_{yy} , and generalized force N_i can be approximated by

$$L(\mathbf{x}_r, \delta_e, \delta_c, \boldsymbol{\eta}) \approx 0.5\rho V^2 s C_L(\alpha, \delta_e, \delta_c, \boldsymbol{\eta}) \quad (7)$$

$$D(\mathbf{x}_r, \delta_e, \delta_c, \boldsymbol{\eta}) \approx 0.5\rho V^2 s C_D(\alpha, \delta_e, \delta_c, \boldsymbol{\eta}) \quad (8)$$

$$T(\mathbf{x}_r, \phi, \boldsymbol{\eta}) \approx 0.5\rho V^2 s [C_{T,\phi}(\alpha)\phi + C_T(\alpha) + \mathbf{C}_T^\eta \boldsymbol{\eta}] \quad (9)$$

$$M_{yy}(\mathbf{x}_r, \phi, \delta_e, \delta_c, \boldsymbol{\eta}) \approx z_T T + 0.5\rho V^2 s \bar{c} C_M(\alpha, \delta_e, \delta_c, \boldsymbol{\eta}) \quad (10)$$

$$N_i(\mathbf{x}_r, \delta_e, \delta_c, \boldsymbol{\eta}) \approx 0.5\rho V^2 s [N_i^{\alpha^2} \alpha^2 + N_i^\alpha \alpha + N_i^{\delta_e} \delta_e + N_i^{\delta_c} \delta_c + N_i^0 + N_i^\eta \boldsymbol{\eta}] \quad (11)$$

where ρ , s , z_T , and \bar{c} represent the air density, reference area, thrust moment arm, and aerodynamic chord, respectively. δ_e stands for the elevator deflection, δ_c stands for the canard deflection, while ϕ represents the fuel equivalence ratio. The aerodynamic coefficients, which are obtained through curve-fitted method, can be expressed as follows:

$$C_L(\alpha, \delta_e, \delta_c, \boldsymbol{\eta}) = C_L^\alpha \alpha + C_L^{\delta_e} \delta_e + C_L^{\delta_c} \delta_c + C_L^0 + \mathbf{C}_L^\eta \boldsymbol{\eta} \quad (12)$$

$$C_D(\alpha, \delta_e, \delta_c, \boldsymbol{\eta}) = C_D^{\alpha^2} \alpha^2 + C_D^\alpha \alpha + C_D^{\delta_e^2} \delta_e^2 + C_D^{\delta_e} \delta_e + C_D^{\delta_c^2} \delta_c^2 + C_D^{\delta_c} \delta_c + C_D^0 + \mathbf{C}_D^\eta \boldsymbol{\eta} \quad (13)$$

$$C_{T,\phi}(\alpha) = C_T^{\phi\alpha^3} \alpha^3 + C_T^{\phi\alpha^2} \alpha^2 + C_T^{\phi\alpha} \alpha + C_T^\phi \quad (14)$$

$$C_T(\alpha) = C_T^3 \alpha^3 + C_T^2 \alpha^2 + C_T^1 \alpha + C_T^0 \quad (15)$$

$$C_M(\alpha, \delta_e, \delta_c, \boldsymbol{\eta}) = C_M^{\alpha^2} \alpha^2 + C_M^\alpha \alpha + C_M^{\delta_e} \delta_e + C_M^{\delta_c} \delta_c + C_M^0 + \mathbf{C}_M^\eta \boldsymbol{\eta} \quad (16)$$

$$\mathbf{C}_j^\eta = [C_j^{\eta_1} \quad 0 \quad C_j^{\eta_2} \quad 0 \quad C_j^{\eta_3} \quad 0], \quad j = T, L, D, M \quad (17)$$

$$N_i^\eta = [N_i^{\eta_1} \quad 0 \quad N_i^{\eta_2} \quad 0 \quad N_i^{\eta_3} \quad 0], \quad i = 1, 2, 3. \quad (18)$$

By introducing a new throttle commanded value ϕ_c , the engine dynamic can be modeled by the following second-order system [49]:

$$\ddot{\phi} = -2\zeta_n \omega_n \dot{\phi} - \omega_n^2 \phi + \omega_n^2 \phi_c \quad (19)$$

where ζ_n represents the engine damping ratio, and ω_n stands for the nominal engine frequency. To increase the fidelity, the limits on the actuator outputs in this study are set as

$$\delta_e \in [-20^\circ, 20^\circ], \quad \phi \in [0.05, 1.5]. \quad (20)$$

For more detailed information about the aerodynamic coefficients of the FAHV, readers can refer to [50].

B. Control Objective

Since the flexible states $\boldsymbol{\eta}$ are hard to obtain in practice, we treat the flexible dynamics as unknown disturbances in our design stage, while the effects of them will be evaluated in simulations [4], [26]. Besides, to cancel the lift-elevator coupling, the canard deflection δ_c is set to be ganged with the elevator deflection δ_e through an interconnect gain $k_{ec} = -C_L^{\delta_e} / C_L^{\delta_c}$. Then, $\delta_c = k_{ec} \delta_e = -(C_L^{\delta_e} / C_L^{\delta_c}) \delta_e$, which indicates that we do not need to treat the canard deflection δ_c as a separate input [57]. Take (1) and (2) as FAHV model outputs. Then, considering measurement noises in the output dynamics, (1)–(5) can be rewritten as follows:

$$\dot{\mathbf{x}}_{out} = \begin{bmatrix} \dot{V} \\ \dot{h} \end{bmatrix} = \begin{bmatrix} \phi_v(\mathbf{x}_r, \boldsymbol{\eta}, \mathbf{u}) \\ \phi_h(\mathbf{x}_r, \boldsymbol{\eta}, \mathbf{u}) \end{bmatrix} = \begin{bmatrix} (T \cos \alpha - D)/m - g \sin \gamma \\ V \sin \gamma \end{bmatrix} \quad (21)$$

$$\dot{\mathbf{x}}_i = \begin{bmatrix} \dot{\gamma} \\ \dot{\alpha} \\ \dot{q} \end{bmatrix} = \begin{bmatrix} (L + T \sin \alpha)/(mV) - g \cos \gamma / V \\ q - \dot{\gamma} \\ M_{yy}/I_{yy} \end{bmatrix} \quad (22)$$

$$\mathbf{y} = \begin{bmatrix} V_m \\ h_m \end{bmatrix} = \mathbf{x}_{out} + \mathbf{w} = \begin{bmatrix} V + w_v \\ h + w_h \end{bmatrix} \quad (23)$$

where $\mathbf{x}_{out} = [V \ h]^T$ represents the output state vector, $\mathbf{x}_i = [\gamma \ \alpha \ q]^T$, and $\mathbf{x}_r = [\mathbf{x}_{out}^T, \mathbf{x}_i^T]^T$. $\mathbf{u} = [\delta_e \ \phi_c]^T$ stands for the control inputs, $\mathbf{y} = [V_m \ h_m]^T$ represents the measured outputs, and $\mathbf{w} = [w_v \ w_h]^T$ stands for the measurement noises in the velocity channel and altitude channel, respectively.

Focusing on the tracking problem in FAHV cruise flight stage, the control objective of this study is to develop a robust control law $\mathbf{u}(\mathbf{y}, \mathbf{x}_i)$ such that in case of noisy measurements \mathbf{y} and unknown disturbances, the output states V and h can track the given reference signals V_c and h_c , respectively.

Throughout this paper, the following assumptions hold:

Assumption 1: w_v and w_h are bounded functions of t . In other words, there exist unknown positive constants w_1 and w_2 such that $|w_v(t)| \leq w_1$ and $|w_h(t)| \leq w_2$.

Assumption 2: V_c together with its derivatives up to the 3rd order and h_c together with its derivatives up to the 4th order are bounded.

III. STATE-ESTIMATOR-INTEGRATED ROBUST ADAPTIVE TRACKING CONTROL DESIGN

In this section, we will describe our robust adaptive tracking control design for FAHV with noisy measurements in detail. First, a continuous-model-based state estimator will be given to estimate the exact states of the velocity and altitude, which are contaminated by measurement noises. Then, based on the noise-free measurements, an ideal state feedback controller will be constructed to fulfill the tracking mission. After combining the state estimator and the controller, the whole robust adaptive tracking control law is finally developed, which is shown in Fig. 2.

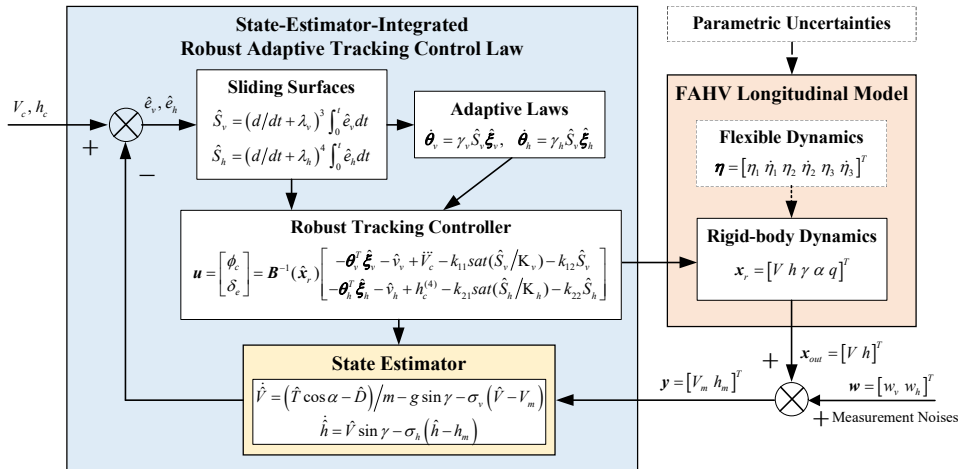


Fig. 2 Overall control scheme.

A. State Estimator Design

To overcome the side effects brought by the measurement noises in the output dynamics, we design the following continuous-model-based state estimator:

$$\begin{aligned}\dot{\hat{V}} &= \phi_{v0}(\hat{\mathbf{x}}_r, \mathbf{u}) - \sigma_v (\hat{V} - V_m) \\ &= (\hat{T} \cos \alpha - \hat{D}) / m - g \sin \gamma - \sigma_v (\hat{V} - V_m)\end{aligned}\quad (24)$$

$$\dot{\hat{h}} = \phi_{h0}(\hat{\mathbf{x}}_r, \mathbf{u}) - \sigma_h (\hat{h} - h_m) = \hat{V} \sin \gamma - \sigma_h (\hat{h} - h_m) \quad (25)$$

where $\hat{\mathbf{x}}_{out} = [\hat{V} \ \hat{h}]^T$ is the estimate of the output states, $\hat{\mathbf{x}}_r = [\hat{\mathbf{x}}_{out}^T, \mathbf{x}_i^T]^T = [\hat{V} \ \hat{h} \ \gamma \ \alpha \ q]^T$, σ_v and σ_h are positive constants,

$$\phi_{v0}(\hat{\mathbf{x}}_r, \mathbf{u}) = (\hat{T} \cos \alpha - \hat{D}) / m - g \sin \gamma \quad (26)$$

$$\phi_{h0}(\hat{\mathbf{x}}_r, \mathbf{u}) = \hat{V} \sin \gamma \quad (27)$$

are nominal models of (21), with

$$\hat{T} = T(\hat{\mathbf{x}}_r, \phi, \mathbf{0}) = 0.5 \rho \hat{V}^2 s [C_{T,\phi}(\alpha) \phi + C_T(\alpha)] \quad (28)$$

$$\hat{D} = D(\hat{\mathbf{x}}_r, \delta_e, \delta_c, \mathbf{0}) = 0.5 \rho \hat{V}^2 s C_D(\alpha, \delta_e, -(C_L^{\delta_e} / C_L^{\delta_c}) \delta_e, \mathbf{0}) \quad (29)$$

while $\mathbf{u} = \mathbf{u}(\hat{\mathbf{x}}_r)$ is the control input which will be developed later. By calculating the integrals of $\dot{\hat{V}}$ and $\dot{\hat{h}}$, the estimate of the output states $\hat{\mathbf{x}}_{out} = [\hat{V} \ \hat{h}]^T$ can be obtained.

Define the estimate error vector as $\tilde{\mathbf{x}}_{out} = [\tilde{V} \ \tilde{h}]^T = \mathbf{x}_{out} - \hat{\mathbf{x}}_{out} = [V - \hat{V} \ h - \hat{h}]^T$. Then, according to (21), (24) and (25), the estimate error dynamics can be written as follows:

$$\begin{aligned}\dot{\tilde{V}} &= \dot{V} - \dot{\hat{V}} \\ &= \phi_v(\mathbf{x}_r, \boldsymbol{\eta}, \mathbf{u}) - (\phi_{v0}(\hat{\mathbf{x}}_r, \mathbf{u}) - \sigma_v (\hat{V} - V_m)) \\ &= \tilde{\phi}_v(\mathbf{x}_r, \boldsymbol{\eta}, \hat{\mathbf{x}}_r) + \sigma_v (\hat{V} - V - w_v) \\ &= -\sigma_v \tilde{V} + \tilde{\phi}_v(\mathbf{x}_r, \boldsymbol{\eta}, \hat{\mathbf{x}}_r) - \sigma_v w_v\end{aligned}\quad (30)$$

$$\begin{aligned}\dot{\tilde{h}} &= \dot{h} - \dot{\hat{h}} \\ &= \phi_h(\mathbf{x}_r, \boldsymbol{\eta}, \mathbf{u}) - (\phi_{h0}(\hat{\mathbf{x}}_r, \mathbf{u}) - \sigma_h (\hat{h} - h_m)) \\ &= \tilde{\phi}_h(\mathbf{x}_r, \boldsymbol{\eta}, \hat{\mathbf{x}}_r) + \sigma_h (\hat{h} - h - w_h) \\ &= -\sigma_h \tilde{h} + \tilde{\phi}_h(\mathbf{x}_r, \boldsymbol{\eta}, \hat{\mathbf{x}}_r) - \sigma_h w_h\end{aligned}\quad (31)$$

where $\tilde{\phi}_v(\mathbf{x}_r, \boldsymbol{\eta}, \hat{\mathbf{x}}_r) = \phi_v(\mathbf{x}_r, \boldsymbol{\eta}, \mathbf{u}) - \phi_{v0}(\hat{\mathbf{x}}_r, \mathbf{u})$ and $\tilde{\phi}_h(\mathbf{x}_r, \boldsymbol{\eta}, \hat{\mathbf{x}}_r) = \phi_h(\mathbf{x}_r, \boldsymbol{\eta}, \mathbf{u}) - \phi_{h0}(\hat{\mathbf{x}}_r, \mathbf{u})$ represent the lumped modeling errors, both of which are globally bounded in $\mathbf{x}_r, \boldsymbol{\eta}$ and $\hat{\mathbf{x}}_r$. Thus, there exist unknown positive constants $\tilde{\Phi}_v$ and $\tilde{\Phi}_h$, such that

$$|\tilde{\phi}_v(\mathbf{x}_r, \boldsymbol{\eta}, \hat{\mathbf{x}}_r)| \leq \tilde{\Phi}_v \quad \text{and} \quad |\tilde{\phi}_h(\mathbf{x}_r, \boldsymbol{\eta}, \hat{\mathbf{x}}_r)| \leq \tilde{\Phi}_h.$$

Now we are going to analyze the stability properties of the state estimator.

Theorem 1: Consider the FAHV longitudinal model (1)–(6), (19) and the state estimator (24) and (25). Then, both the estimate errors \tilde{V} and \tilde{h} are semi globally bounded.

Proof: Consider the following Lyapunov function candidate:

$$V_1 = V_{1v} + V_{1h} = \tilde{V}^2 + \tilde{h}^2. \quad (32)$$

Differentiating V_1 along the system trajectory, we can obtain

$$\begin{aligned} \dot{V}_1 &= \dot{V}_{1v} + \dot{V}_{1h} \\ &= 2\tilde{V}\dot{\tilde{V}} + 2\tilde{h}\dot{\tilde{h}} \\ &= 2\tilde{V}\left(-\sigma_v\tilde{V} + \tilde{\phi}_v(\mathbf{x}_r, \boldsymbol{\eta}, \hat{\mathbf{x}}_r) - \sigma_v w_v\right) \\ &\quad + 2\tilde{h}\left(-\sigma_h\tilde{h} + \tilde{\phi}_h(\mathbf{x}_r, \boldsymbol{\eta}, \hat{\mathbf{x}}_r) - \sigma_h w_h\right) \\ &= -2\sigma_v\tilde{V}^2 + 2\tilde{V}\tilde{\phi}_v(\mathbf{x}_r, \boldsymbol{\eta}, \hat{\mathbf{x}}_r) - 2\sigma_v\tilde{V}w_v \\ &\quad - 2\sigma_h\tilde{h}^2 + 2\tilde{h}\tilde{\phi}_h(\mathbf{x}_r, \boldsymbol{\eta}, \hat{\mathbf{x}}_r) - 2\sigma_h\tilde{h}w_h \\ &\leq -2\sigma_v\tilde{V}^2 + 2|\tilde{V}|\tilde{\Phi}_v + 2\sigma_v|\tilde{V}|w_1 - 2\sigma_h\tilde{h}^2 + 2|\tilde{h}|\tilde{\Phi}_h \\ &\quad + 2\sigma_h|\tilde{h}|w_2. \end{aligned} \quad (33)$$

If we let

$$-2\sigma_v\tilde{V}^2 + 2|\tilde{V}|\tilde{\Phi}_v + 2\sigma_v|\tilde{V}|w_1 \leq -\sigma_v V_{1v} \quad (34)$$

$$-2\sigma_h\tilde{h}^2 + 2|\tilde{h}|\tilde{\Phi}_h + 2\sigma_h|\tilde{h}|w_2 \leq -\sigma_h V_{1h} \quad (35)$$

then

$$\dot{V}_1 \leq -\sigma V_1 \quad (36)$$

can be satisfied, where $\sigma = \min(\sigma_v, \sigma_h)$. Solving inequalities (34) and (35), we have

$$V_{1v} \geq \left(2\tilde{\Phi}_v/\sigma_v + 2w_1\right)^2 \quad (37)$$

$$V_{1h} \geq \left(2\tilde{\Phi}_h/\sigma_h + 2w_2\right)^2. \quad (38)$$

Therefore, the estimate errors \tilde{V} and \tilde{h} are invariant to the following sets

$$\Sigma_v = \left\{|\tilde{V}| \leq 2\tilde{\Phi}_v/\sigma_v + 2w_1\right\} \quad (39)$$

$$\Sigma_h = \left\{|\tilde{h}| \leq 2\tilde{\Phi}_h/\sigma_h + 2w_2\right\} \quad (40)$$

respectively, which indicates the semi global boundedness of \tilde{V} and \tilde{h} . This completes the proof. \square

Remark 1: According to (39) and (40), it can be found that with fixed σ_v and σ_h , both the boundaries of the estimate errors \tilde{V} and \tilde{h} consist of two parts: one is the modeling error between the nominal model and the truth model corresponding to the terms $\tilde{\Phi}_v$ and $\tilde{\Phi}_h$, which mainly results from the unknown flexible dynamics, parametric uncertainties and other model disturbances. The other is the effect of the measurement noises. In the case where the measurement noises are absent, we can obtain

$$\lim_{\sigma_v \rightarrow \infty} |\tilde{V}| \leq \lim_{\sigma_v \rightarrow \infty} \left(2\tilde{\Phi}_v/\sigma_v\right) = 0 \quad (41)$$

$$\lim_{\sigma_h \rightarrow \infty} |\tilde{h}| \leq \lim_{\sigma_h \rightarrow \infty} \left(2\tilde{\Phi}_h/\sigma_h\right) = 0 \quad (42)$$

which means that we can minify the estimate errors \tilde{V} and \tilde{h} by choosing larger gains σ_v and σ_h respectively in this case.

Remark 2: When measurement noises exist, for the proposed state estimator (24) and (25), if we choose $\phi_{v0}(\hat{\mathbf{x}}_r, \mathbf{u}) = 0$ and $\phi_{h0}(\hat{\mathbf{x}}_r, \mathbf{u}) = 0$, after Laplace transformation, we can obtain the relationships between \hat{V} , \hat{h} and V_m , h_m in the Laplace domain as follows:

$$H_v(s) = \frac{\hat{V}(s)}{V_m(s)} = \frac{1}{(1/\sigma_v)s + 1} \quad (43)$$

$$H_h(s) = \frac{\hat{H}(s)}{H_m(s)} = \frac{1}{(1/\sigma_h)s + 1} \quad (44)$$

which are common first-order LPFs. In this case, $\tilde{\phi}_v(\mathbf{x}_r, \boldsymbol{\eta}, \hat{\mathbf{x}}_r) = \phi_v(\mathbf{x}_r, \boldsymbol{\eta}, \mathbf{u})$ and $\tilde{\phi}_h(\mathbf{x}_r, \boldsymbol{\eta}, \hat{\mathbf{x}}_r) = \phi_h(\mathbf{x}_r, \boldsymbol{\eta}, \mathbf{u})$, which mean the derivatives of the velocity and altitude of FAHV, respectively. In the steady-state process, $\tilde{\phi}_v(\mathbf{x}_r, \boldsymbol{\eta}, \hat{\mathbf{x}}_r) = \tilde{\phi}_h(\mathbf{x}_r, \boldsymbol{\eta}, \hat{\mathbf{x}}_r) = 0$, which indicates no modeling errors exist so that the estimate errors \tilde{V} and \tilde{h} are only affected by the measurement noises. However, in the transition process where the reference signals change, larger bounds of $\tilde{\Phi}_v$ and $\tilde{\Phi}_h$ will be brought in by LPFs (43) and (44). Compared with (24) and (25), if we choose the same σ_v and σ_h , larger estimate errors will emerge, which will greatly deteriorate the tracking performances and even make the close-loop system broken down. Therefore, for LPFs, we need to choose larger σ_v and σ_h to reduce the effects of $\tilde{\Phi}_v$ and $\tilde{\Phi}_h$ although it actually leads to a sacrifice of high-frequency filtering property.

B. Ideal State Feedback Tracking Control Design

1) Brief Description of IT2-FLS

To identify the unknown nonlinear dynamics of FAHV, we employ IT2-FLS which was brought out by Zadeh in 1970s [51] in this study. A typical IT2-FLS is usually composed of the following five parts: fuzzifier, rule bases, inference, type reducer, and defuzzifier, which can be seen in Fig. 3. As an extension of type-1 fuzzy logic system (T1-FLS), IT2-FLS is more appreciated in dealing with uncertain parameters and unmodeled dynamics due to the extra degree of freedom provided by interval type-2 fuzzy sets (IT2-FSs) (Fig. 4), which means a better capability of IT2-FLS in modeling unreliable information.

Fig. 3 Interval type-2 fuzzy logic system.

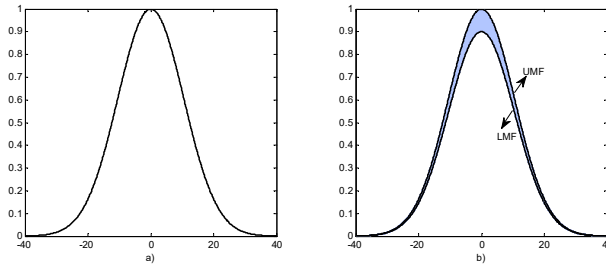


Fig. 4 a) Type-1 fuzzy set and b) interval type-2 fuzzy set.

Considering an n -inputs-one-output Mamdani IT2-FLS, the s th rule of the rule bases has the following form:

$$\begin{aligned} \text{Rule } s : & \text{ If } x_{f_1} \text{ is } \tilde{F}_1^s \text{ and } x_{f_2} \text{ is } \tilde{F}_2^s \dots \text{ and } x_{f_n} \text{ is } \tilde{F}_n^s \\ & \text{ Then } u \text{ is } \tilde{G}^s \quad s = 1, 2, \dots, M \end{aligned} \quad (45)$$

where $\mathbf{x}_f = [x_{f_1}, x_{f_2}, \dots, x_{f_n}]^T \in \mathbf{R}^n$ is the input vector and $u \in R$ is the output of the IT2-FLS. Besides, \tilde{F}_i^s ($i = 1, 2, \dots, n$) is

the antecedent IT2-FS, with lower membership function (LMF) $\underline{\mu}_{\tilde{F}_i^s}(x_{f_i})$ and upper membership function (UMF) $\overline{\mu}_{\tilde{F}_i^s}(x_{f_i})$, while \tilde{G}^s is the consequent IT2-FS, with corresponding centroids of $[\theta_i^s, \theta_r^s]$. Then, if we apply singleton fuzzification and product inference, the degree of firing $f^s(\mathbf{x}_f)$ satisfies the following relationship:

$$f^s(\mathbf{x}_f) \in \left[\underline{f}^s(\mathbf{x}_f), \overline{f}^s(\mathbf{x}_f) \right] \\ = \left[\prod_{i=1}^n \underline{\mu}_{\tilde{F}_i^s}(x_{f_i}), \prod_{i=1}^n \overline{\mu}_{\tilde{F}_i^s}(x_{f_i}) \right]. \quad (46)$$

Let

$$\xi^s(\mathbf{x}_f) = f^s(\mathbf{x}_f) \Big/ \sum_{s=1}^M f^s(\mathbf{x}_f) \quad (47)$$

denotes the fuzzy basic function (FBF). Then, the left and right boundary FBF vectors $\underline{\xi}_l(\mathbf{x}_f) = [\xi_l^1(\mathbf{x}_f), \xi_l^2(\mathbf{x}_f), \dots, \xi_l^n(\mathbf{x}_f)]^T$ and $\underline{\xi}_r(\mathbf{x}_f) = [\xi_r^1(\mathbf{x}_f), \xi_r^2(\mathbf{x}_f), \dots, \xi_r^n(\mathbf{x}_f)]^T$ can be obtained through Karnik-Mendel algorithm [55], which can be further used to calculate the left and right end points of the type-reduced interval type-1 fuzzy set u_l and u_r under center-of-sets type reduction:

$$u_l(\mathbf{x}_f) = \theta_l^T \underline{\xi}_l(\mathbf{x}_f), \quad u_r(\mathbf{x}_f) = \theta_r^T \underline{\xi}_r(\mathbf{x}_f) \quad (48)$$

where $\theta_l = [\theta_l^1, \theta_l^2, \dots, \theta_l^M]^T$ and $\theta_r = [\theta_r^1, \theta_r^2, \dots, \theta_r^M]^T$. Finally, the crisp output $u(\mathbf{x}_f)$ can be obtained through center average defuzzification:

$$u(\mathbf{x}_f) = 0.5(u_l(\mathbf{x}_f) + u_r(\mathbf{x}_f)) \\ = 0.5(\theta_l^T \underline{\xi}_l(\mathbf{x}_f) + \theta_r^T \underline{\xi}_r(\mathbf{x}_f)) = \theta^T \underline{\xi}(\mathbf{x}_f) \quad (49)$$

where $\theta = 0.5[\theta_l, \theta_r]^T$ and $\underline{\xi}(\mathbf{x}_f) = [\underline{\xi}_l(\mathbf{x}_f), \underline{\xi}_r(\mathbf{x}_f)]^T$.

The following lemma demonstrates the Mamdani IT2-FLS's capability of approximating a real continuous function on a compact domain.

Lemma 1 [52]: The Mamdani IT2-FLS can uniformly approximate any real continuous function $f(\mathbf{x}): \mathbf{R}^n \rightarrow \mathbf{R}$ in a compact set $\Xi \in \mathbf{R}^n$ to any degree of accuracy. In other words, for $\forall \varepsilon > 0$, there exists a Mamdani IT2-FLS as (49) such that

$$\sup_{\mathbf{x} \in \Xi} |f(\mathbf{x}) - \theta^T \underline{\xi}(\mathbf{x})| < \varepsilon. \quad (50)$$

Therefore, the real continuous function $f(\mathbf{x})$ can be expressed as follows:

$$f(\mathbf{x}) = \theta^{*T} \underline{\xi}(\mathbf{x}) + \varepsilon_{\min} \quad (51)$$

where θ^* denotes the optimal parameter estimation, which can be defined as follows:

$$\theta^* = \arg \min_{\theta \in \mathbf{R}^M} \left\{ \sup_{\mathbf{x} \in \Xi} |f(\mathbf{x}) - \theta^T \underline{\xi}(\mathbf{x})| \right\} \quad (52)$$

while ε_{\min} represents the minimal estimation error.

2) Ideal Robust Adaptive Tracking Control Design

Facing the control objective, an ideal state feedback tracking control law $\mathbf{u} = \mathbf{u}(\mathbf{x}_f)$ will be developed for FAHV to tackle the tracking problems in this part. Based on differential geometric control theory [53], the FAHV longitudinal model can be transformed into the following affine nonlinear form by differentiating V and h three times and four times separately:

$$\begin{bmatrix} \ddot{V} \\ h^{(4)} \end{bmatrix} = \begin{bmatrix} f_1 \\ f_2 \end{bmatrix} + \begin{bmatrix} b_{11} & b_{12} \\ b_{21} & b_{22} \end{bmatrix} \begin{bmatrix} \phi_c \\ \delta_e \end{bmatrix} \quad (53)$$

where

$$f_1 = (\omega_1 \ddot{x}_0 + \dot{x}^T \Omega_2 \dot{x}) / m \quad (54)$$

$$\begin{aligned} f_2 = & (\omega_1 \ddot{x}_0 + \dot{x}^T \Omega_2 \dot{x}) \sin \gamma / m + V (\pi_1 \ddot{x}_0 + \dot{x}^T \Pi_2 \dot{x}) \cos \gamma \\ & + 3\ddot{V} \dot{\gamma} \cos \gamma - 3\dot{V} \dot{\gamma}^2 \sin \gamma + 3\dot{V} \ddot{\gamma} \cos \gamma \\ & - 3V \dot{\gamma} \ddot{\gamma} \sin \gamma - V \dot{\gamma}^3 \cos \gamma \end{aligned} \quad (55)$$

$$b_{11} = \frac{\omega_n^2}{m} \frac{\partial T}{\partial \phi} \cos \alpha \quad (56)$$

$$b_{12} = \frac{\rho V^2 s \bar{c}}{2m I_{yy}} \left(\frac{\partial T}{\partial \alpha} \cos \alpha - T \sin \alpha - \frac{\partial D}{\partial \alpha} \right) \left(C_M^{\delta_e} - \frac{C_L^{\delta_e}}{C_L^{\delta_c}} C_M^{\delta_c} \right) \quad (57)$$

$$b_{21} = \frac{\omega_n^2}{m} \frac{\partial T}{\partial \phi} \sin(\gamma + \alpha) \quad (58)$$

$$\begin{aligned} b_{22} = & \frac{\rho V^2 s \bar{c}}{2m I_{yy}} \left[\left(\frac{\partial T}{\partial \alpha} \cos \alpha - T \sin \alpha - \frac{\partial D}{\partial \alpha} \right) \sin \gamma \right. \\ & \left. + \left(\frac{\partial L}{\partial \alpha} + \frac{\partial T}{\partial \alpha} \sin \alpha + T \cos \alpha \right) \cos \gamma \right] \left(C_M^{\delta_e} - \frac{C_L^{\delta_e}}{C_L^{\delta_c}} C_M^{\delta_c} \right). \end{aligned} \quad (59)$$

The detailed expressions of \mathbf{x} , \ddot{x}_0 , ω_1 , Ω_2 , π_1 and Π_2 are given in the Appendix.

However, large flight envelope and severe environmental changes will inevitably cause aerodynamic parametric uncertainties, which may directly affect the system stability as well as the flight safety. Thus, taking parametric uncertainties into consideration, we have

$$\begin{aligned} \begin{bmatrix} \ddot{V} \\ h^{(4)} \end{bmatrix} &= \begin{bmatrix} f_1 + \Delta f_1 \\ f_2 + \Delta f_2 \end{bmatrix} + \begin{bmatrix} b_{11} + \Delta b_{11} & b_{12} + \Delta b_{12} \\ b_{21} + \Delta b_{21} & b_{22} + \Delta b_{22} \end{bmatrix} \begin{bmatrix} \phi_c \\ \delta_e \end{bmatrix} \\ &= \begin{bmatrix} f_v \\ f_h \end{bmatrix} + \begin{bmatrix} b_{11} & b_{12} \\ b_{21} & b_{22} \end{bmatrix} \begin{bmatrix} \phi_c \\ \delta_e \end{bmatrix} \\ &= \mathbf{F}(\mathbf{x}_r) + \mathbf{B}(\mathbf{x}_r) \mathbf{u} \end{aligned} \quad (60)$$

where

$$\mathbf{F}(\mathbf{x}_r) = \begin{bmatrix} f_v \\ f_h \end{bmatrix} = \begin{bmatrix} f_1 + \Delta f_1 \\ f_2 + \Delta f_2 \end{bmatrix} + \begin{bmatrix} \Delta b_{11} & \Delta b_{12} \\ \Delta b_{21} & \Delta b_{22} \end{bmatrix} \begin{bmatrix} \phi_c \\ \delta_e \end{bmatrix} \quad (61)$$

is an uncertainty-embedded vector,

$$\mathbf{B}(\mathbf{x}_r) = \begin{bmatrix} b_{11}(\mathbf{x}_r) & b_{12}(\mathbf{x}_r) \\ b_{21}(\mathbf{x}_r) & b_{22}(\mathbf{x}_r) \end{bmatrix} \quad (62)$$

is the input gain matrix which is supposed to be invertible [54], while Δf_1 , Δf_2 , Δb_{11} , Δb_{12} , Δb_{21} and Δb_{22} are corresponding lumped uncertain terms.

Define the velocity tracking error and altitude tracking error as $e_v = V - V_c$ and $e_h = h - h_c$, respectively. Then, the sliding surfaces of the velocity and altitude can be designed as follows:

$$S_v = (d/dt + \lambda_v)^3 \int_0^t e_v dt \quad (63)$$

$$S_h = (d/dt + \lambda_h)^4 \int_0^t e_h dt \quad (64)$$

where λ_v and λ_h are positive constants. Differentiating (63) and (64), we can obtain the following relationship:

$$\begin{bmatrix} \dot{S}_v \\ \dot{S}_h \end{bmatrix} = \begin{bmatrix} v_v - \ddot{V}_c \\ v_h - h_c^{(4)} \end{bmatrix} + \mathbf{F}(\mathbf{x}_r) + \mathbf{B}(\mathbf{x}_r) \mathbf{u} \quad (65)$$

where

$$v_v = \lambda_v^3 e_v + 3\lambda_v^2 \dot{e}_v + 3\lambda_v \ddot{e}_v \quad (66)$$

$$v_h = \lambda_h^4 e_h + 4\lambda_h^3 \dot{e}_h + 6\lambda_h^2 \ddot{e}_h + 4\lambda_h \dddot{e}_h \quad (67)$$

are two terms associated with the velocity tracking error and altitude tracking error, respectively.

Since the precise expressions of f_v and f_h are both unavailable, here we utilize two IT2-FLSs to approximate these two terms respectively. Then we have

$$\hat{f}_v = \boldsymbol{\theta}_v^T \boldsymbol{\xi}_v(\mathbf{x}_r), \quad \hat{f}_h = \boldsymbol{\theta}_h^T \boldsymbol{\xi}_h(\mathbf{x}_r). \quad (68)$$

The ideal state feedback tracking control law can be designed as follows:

$$\mathbf{u} = \mathbf{B}^{-1}(\mathbf{x}_r) \begin{bmatrix} -\boldsymbol{\theta}_v^T \boldsymbol{\xi}_v - v_v + \ddot{V}_c - k_{11} \text{sgn}(S_v) - k_{12} S_v \\ -\boldsymbol{\theta}_h^T \boldsymbol{\xi}_h - v_h + h_c^{(4)} - k_{21} \text{sgn}(S_h) - k_{22} S_h \end{bmatrix} \quad (69)$$

where $k_{11}, k_{12}, k_{21}, k_{22} > 0$, and the adaptive laws are

$$\dot{\boldsymbol{\theta}}_v = \gamma_v S_v \boldsymbol{\xi}_v, \quad \dot{\boldsymbol{\theta}}_h = \gamma_h S_h \boldsymbol{\xi}_h \quad (70)$$

where $\gamma_v, \gamma_h > 0$. Then, the stability properties of the proposed state feedback control law are given as follows.

Theorem 2: Consider the FAHV longitudinal model (1)–(6), (19) together with the state feedback control input (69) and the adaptive laws (70). Then, the sliding surfaces in the state feedback system S_v and S_h are semi globally bounded.

Proof: According to (51), the uncertain terms f_v and f_h can be expressed as follows:

$$f_v = \boldsymbol{\theta}_v^{*T} \boldsymbol{\xi}_v + \varepsilon_{\min,v}, \quad f_h = \boldsymbol{\theta}_h^{*T} \boldsymbol{\xi}_h + \varepsilon_{\min,h}. \quad (71)$$

Then, substituting (69) and (71) into (65), it becomes

$$\begin{bmatrix} \dot{S}_v \\ \dot{S}_h \end{bmatrix} = \begin{bmatrix} \tilde{\boldsymbol{\theta}}_v^T \boldsymbol{\xi}_v + \varepsilon_{\min,v} - k_{11} \text{sgn}(S_v) - k_{12} S_v \\ \tilde{\boldsymbol{\theta}}_h^T \boldsymbol{\xi}_h + \varepsilon_{\min,h} - k_{21} \text{sgn}(S_h) - k_{22} S_h \end{bmatrix} \quad (72)$$

where $\tilde{\boldsymbol{\theta}}_v = \boldsymbol{\theta}_v^* - \boldsymbol{\theta}_v$ and $\tilde{\boldsymbol{\theta}}_h = \boldsymbol{\theta}_h^* - \boldsymbol{\theta}_h$.

Consider the following Lyapunov function candidate:

$$V_2 = \frac{1}{2} S_v^2 + \frac{1}{2} S_h^2 + \frac{1}{2\gamma_v} \tilde{\boldsymbol{\theta}}_v^T \tilde{\boldsymbol{\theta}}_v + \frac{1}{2\gamma_h} \tilde{\boldsymbol{\theta}}_h^T \tilde{\boldsymbol{\theta}}_h. \quad (73)$$

The time derivative of V_2 along the system trajectory is

$$\begin{aligned} \dot{V}_2 &= S_v \dot{S}_v + S_h \dot{S}_h + \frac{1}{\gamma_v} \tilde{\boldsymbol{\theta}}_v^T \dot{\tilde{\boldsymbol{\theta}}}_v + \frac{1}{\gamma_h} \tilde{\boldsymbol{\theta}}_h^T \dot{\tilde{\boldsymbol{\theta}}}_h \\ &= S_v \left(-k_{11} \text{sgn}(S_v) - k_{12} S_v + \varepsilon_{\min,v} \right) \\ &\quad + S_h \left(-k_{21} \text{sgn}(S_h) - k_{22} S_h + \varepsilon_{\min,h} \right) \\ &\quad + \tilde{\boldsymbol{\theta}}_v^T \left(S_v \boldsymbol{\xi}_v - \frac{1}{\gamma_v} \dot{\tilde{\boldsymbol{\theta}}}_v \right) + \tilde{\boldsymbol{\theta}}_h^T \left(S_h \boldsymbol{\xi}_h - \frac{1}{\gamma_h} \dot{\tilde{\boldsymbol{\theta}}}_h \right). \end{aligned} \quad (74)$$

Substituting (70) into (74), \dot{V}_2 becomes

$$\begin{aligned} \dot{V}_2 &= -k_{11}|S_v| - k_{12}S_v^2 - k_{21}|S_h| - k_{22}S_h^2 + S_v\varepsilon_{\min,v} \\ &\quad + S_h\varepsilon_{\min,h} \\ &\leq |S_v|(-k_{12}|S_v| - k_{11} + |\varepsilon_{\min,v}|) \\ &\quad + |S_h|(-k_{22}|S_h| - k_{21} + |\varepsilon_{\min,h}|). \end{aligned} \quad (75)$$

Therefore, S_v and S_h are invariant to the following sets

$$\Xi_v = \left\{ |S_v| \leq \max \left\{ \frac{-k_{11} + |\varepsilon_{\min,v}|}{k_{12}}, 0 \right\} \right\} \quad (76)$$

$$\Xi_h = \left\{ |S_h| \leq \max \left\{ \frac{-k_{21} + |\varepsilon_{\min,h}|}{k_{22}}, 0 \right\} \right\} \quad (77)$$

respectively, which completes the proof. \square

Remark 3: Although Theorem 2 has analyzed the boundedness of the sliding surfaces S_v and S_h , it is still a conservative result because with favorable design of IT2-FLSs, the unknown terms $|\varepsilon_{\min,v}|$ and $|\varepsilon_{\min,h}|$ can be actually very small. Thus, if comparatively large positive k_{11} and k_{21} are taken, which satisfy $k_{11} > |\varepsilon_{\min,v}|$ and $k_{21} > |\varepsilon_{\min,h}|$, then we can obtain

$$\Xi_v = \{|S_v| = 0\}, \quad \Xi_h = \{|S_h| = 0\} \quad (78)$$

which indicates that the tracking errors of the velocity and altitude can converge to zero in the ideal state feedback case.

Remark 4: To avoid chattering problems brought by the discontinuous function $\text{sgn}(x)$, here we replace $\text{sgn}(x)$ with a continuous saturation function $\text{sat}(x)$, where

$$\text{sat}(x) = \begin{cases} x, & \text{if } |x| \leq 1 \\ \text{sgn}(x), & \text{otherwise} \end{cases} \quad (79)$$

Then the control law (69) becomes:

$$\mathbf{u} = \mathbf{B}^{-1}(\mathbf{x}_r) \begin{bmatrix} -\boldsymbol{\theta}_v^T \boldsymbol{\xi}_v - v_v + \ddot{V}_c - k_{11}\text{sat}(S_v/K_v) - k_{12}S_v \\ -\boldsymbol{\theta}_h^T \boldsymbol{\xi}_h - v_h + h_c^{(4)} - k_{21}\text{sat}(S_h/K_h) - k_{22}S_h \end{bmatrix} \quad (80)$$

where K_v and K_h are positive constants.

C. Control Synthesis

In the previous subsections, we have separately finished the design of the state estimator and the ideal state feedback tracking controller. In this subsection, we will combine these two parts through substituting the noise-free measurement vector \mathbf{x}_r in (80) by its estimate one $\hat{\mathbf{x}}_r$ [9], [53], and [56]. Finally, the whole state-estimator-integrated robust adaptive tracking control law can be written as follows:

$$\begin{aligned} \mathbf{u} &= [\phi_c \quad \delta_c]^T \\ &= \mathbf{B}^{-1}(\hat{\mathbf{x}}_r) \begin{bmatrix} -\boldsymbol{\theta}_v^T \hat{\boldsymbol{\xi}}_v - \hat{v}_v + \ddot{V}_c - k_{11}\text{sat}(\hat{S}_v/K_v) - k_{12}\hat{S}_v \\ -\boldsymbol{\theta}_h^T \hat{\boldsymbol{\xi}}_h - \hat{v}_h + h_c^{(4)} - k_{21}\text{sat}(\hat{S}_h/K_h) - k_{22}\hat{S}_h \end{bmatrix} \end{aligned} \quad (81)$$

$$\hat{S}_v = (d/dt + \lambda_v)^3 \int_0^t \hat{e}_v dt \quad (82)$$

$$\hat{S}_h = (d/dt + \lambda_h)^4 \int_0^t \hat{e}_h dt \quad (83)$$

$$\hat{v}_v = \lambda_v^3 \hat{e}_v + 3\lambda_v^2 \dot{\hat{e}}_v + 3\lambda_v \ddot{\hat{e}}_v \quad (84)$$

$$\hat{v}_h = \lambda_h^4 \hat{e}_h + 4\lambda_h^3 \dot{\hat{e}}_h + 6\lambda_h^2 \ddot{\hat{e}}_h + 4\lambda_h \dddot{\hat{e}}_h \quad (85)$$

$$\begin{aligned} \dot{\hat{V}} &= \phi_{v0}(\hat{\mathbf{x}}_r, \mathbf{u}) - \sigma_v (\hat{V} - V_m) \\ &= (\hat{T} \cos \alpha - \hat{D}) / m - g \sin \gamma - \sigma_v (\hat{V} - V_m) \end{aligned} \quad (86)$$

$$\dot{\hat{h}} = \phi_{h0}(\hat{\mathbf{x}}_r, \mathbf{u}) - \sigma_h (\hat{h} - h_m) = \hat{V} \sin \gamma - \sigma_h (\hat{h} - h_m) \quad (87)$$

$$\hat{T} = 0.5 \rho \hat{V}^2 s [C_{T,\phi}(\alpha) \phi + C_T(\alpha)] \quad (88)$$

$$\hat{D} = 0.5 \rho \hat{V}^2 s C_D(\alpha, \delta_e, -(C_L^{\delta_e} / C_L^{\delta_c}) \delta_e, \mathbf{0}) \quad (89)$$

$$\dot{\hat{\theta}}_v = \gamma_v \hat{S}_v \hat{\xi}_v, \quad \dot{\hat{\theta}}_h = \gamma_h \hat{S}_h \hat{\xi}_h \quad (90)$$

where $\hat{\xi}_v = \xi_v(\hat{\mathbf{x}}_r)$, $\hat{\xi}_h = \xi_h(\hat{\mathbf{x}}_r)$, $\hat{\mathbf{x}}_r = [\hat{\mathbf{x}}_{out}^T, \mathbf{x}_i^T]^T = [\hat{V} \hat{h} \gamma \alpha q]^T$, $\hat{e}_v = \hat{V} - V_c$, $\hat{e}_h = \hat{h} - h_c$. $k_{11}, k_{12}, k_{21}, k_{22}, K_v, K_h, \lambda_v, \lambda_h, \sigma_v, \sigma_h, \gamma_v$ and γ_h are positive constants.

IV. NUMERICAL SIMULATIONS

In this section, four scenarios are considered to verify the effectiveness of the proposed state-estimator-integrated robust adaptive tracking control law (81)–(90). The trim conditions of FAHV are listed in TABLE I. Reference signals V_c and h_c together with their high-order derivatives are generated by passing step signals 91.44 m/s and 1219.2 m through the following tracking differentiators, respectively:

$$\begin{cases} f_{s1}(N) = -\kappa_v (\kappa_v (V_c(N) - V_r) + 3\dot{V}_c(N)) + 3\ddot{V}_c(N) \\ V_c(N+1) = V_c(N) + \tau * \dot{V}_c(N) \\ \dot{V}_c(N+1) = \dot{V}_c(N) + \tau * \ddot{V}_c(N) \\ \ddot{V}_c(N+1) = \ddot{V}_c(N) + \tau * f_{s1}(N) \end{cases} \quad (91)$$

$$\begin{cases} f_{s2}(N) = -\kappa_h (\kappa_h (h_c(N) - h_r) + 4\dot{h}_c(N) + 6\ddot{h}_c(N) + 4\dddot{h}_c(N)) \\ h_c(N+1) = h_c(N) + \tau * \dot{h}_c(N) \\ \dot{h}_c(N+1) = \dot{h}_c(N) + \tau * \ddot{h}_c(N) \\ \ddot{h}_c(N+1) = \ddot{h}_c(N) + \tau * \dddot{h}_c(N) \\ \dddot{h}_c(N+1) = \dddot{h}_c(N) + \tau * f_{s2}(N) \end{cases} \quad (92)$$

where N is the number of iteration, κ_v and κ_h are the “velocity factors” which are related with the speed of the arranged transition process, and τ is the time step. Here we choose $\kappa_v = \kappa_h = 0.2$ and $\tau = 0.01$.

For both two IT2-FLSSs, \hat{e}_v and \hat{e}_h are chosen as the inputs. All the antecedent fuzzy sets are set as Gaussian IT2-FSSs, with the following LMF and UMF:

$$\begin{cases} \underline{\mu}_{\hat{F}_i^s}(\hat{e}_i) = 0.9 \times \exp\left(-\left(\hat{e}_i - m_{\hat{F}_i^s}\right)^2 / \left(2\sigma_{\hat{F}_i^s}^2\right)\right) \\ \bar{\mu}_{\hat{F}_i^s}(\hat{e}_i) = \exp\left(-\left(\hat{e}_i - m_{\hat{F}_i^s}\right)^2 / \left(2\sigma_{\hat{F}_i^s}^2\right)\right) \end{cases} \quad i = v, h \quad (93)$$

respectively. \hat{e}_v and \hat{e}_h each have five antecedent fuzzy sets, with their centers $m_{\hat{F}_i^s}$ being evenly spaced in $[-60, 60] \times [-80, 80]$. Besides, $\sigma_{\hat{F}_i^s} = 10.5$ is taken. Thus, in each IT2-FLS, there are 25 rules in total. Other control parameters are given in TABLE II.

TABLE I
TRIM CONDITIONS

Rigid-body states	Value	Flexible states	Value
V	2391.58 m/s	η_1	0.594
h	25908 m	η_2	-0.0976
γ	0 rad	η_3	-0.0335
α	0.0219 rad	$\dot{\eta}_1$	0
q	0 rad/s	$\dot{\eta}_2$	0
		$\dot{\eta}_3$	0

TABLE II
CONTROL PARAMETERS

Parameters	Value	Parameters	Value
k_{11}	6	k_{12}	11
k_{21}	5.5	k_{22}	10.5
K_v	1.5	K_h	2
λ_v	2.35	λ_h	1.05
σ_v	0.8	σ_h	0.02
γ_v	500	γ_h	150

To better show the superiorities of our proposed robust adaptive control system (labeled as ‘‘RAC-Sys’’ in the figures), other four counterparts with different state estimators are evaluated in the first three scenarios, while in the last scenario the method in [48] is taken as a comparison. The first counterpart uses no state estimator (labeled as ‘‘No-SE-Sys’’ in the figures), which means that the noise-contaminated states will be directly fed into the controller. The second and third ones take two sets of specified LPFs as (43) and (44) in the feedback channel. For the second counterpart (labeled as ‘‘LPF1-Sys’’ in the figures), $\sigma_v = 0.8$ and $\sigma_h = 0.02$ are chosen, which are the same as the ones in the proposed state estimator, while for the third (labeled as ‘‘LPF2-Sys’’ in the figures), $\sigma_v = 20/3$ and $\sigma_h = 2.5$ are taken, which are actually larger ones. The fourth counterpart utilizes an UKF for state estimation (labeled as ‘‘UKF-Sys’’ in the figures). Moreover, according to [29], the measurement noises are generated by Simulink’s ‘‘Gaussian Noise Generator’’ block, which guarantees that in each scenario, the measurement noises can keep the same for all the comparisons.

Scenario 1: In the first scenario, the measurement noises are absent. The simulation results are shown in Fig. 5-7. From Fig. 5 we can find that, LPF1-Sys breaks down at about 10s. Besides, both the velocity and altitude tracking errors of UKF-Sys cannot converge near 0. Except for LPF1-Sys and UKF-Sys, all the other three systems can successfully track the given reference signals. In addition, No-SE-Sys has the best tracking performances in both the velocity channel and altitude channel. Although our proposed RAC-Sys has small tracking errors in both two channels in the steady-state process, which are brought by the modeling errors in the state estimator, in the transition process they are explicitly smaller than those of LPF2-Sys. Fig. 6 depicts the results of the velocity and altitude estimates. We can see that, because of fast changing of the reference signals, small σ_v and σ_h in LPF1-Sys can lead to large estimate errors at the start of the simulation, which finally result in a flight failure, while for LPF2-Sys, large σ_v and σ_h are able to keep the close-loop system stable, which is consistent with the analyses in Remark 2. Besides, a severe deterioration of UKF performance occurs due to the unknown flexible dynamics. Moreover, due to the embedded nominal model terms $\phi_{v0}(\hat{x}_r, \mathbf{u})$ and $\phi_{h0}(\hat{x}_r, \mathbf{u})$, our RAC-Sys has the smallest estimate errors in the transition process. The control inputs are presented in Fig. 7, which indicates that when the measurement noises are absent, the actuators of No-SE-Sys, LPF2-Sys, UKF-Sys and RAC-Sys perform almost the same.

Furthermore, integral of square error (ISE) and integral of the absolute value of the error (IAE) are utilized here to evaluate the tracking performances, while root mean square error (RMSE) is employed to evaluate the estimate performances. The results can be seen in TABLE III. It is easy to see that, No-SE-Sys shows the best tracking performances, while our proposed RAC-Sys has the best estimate performances in this scenario.

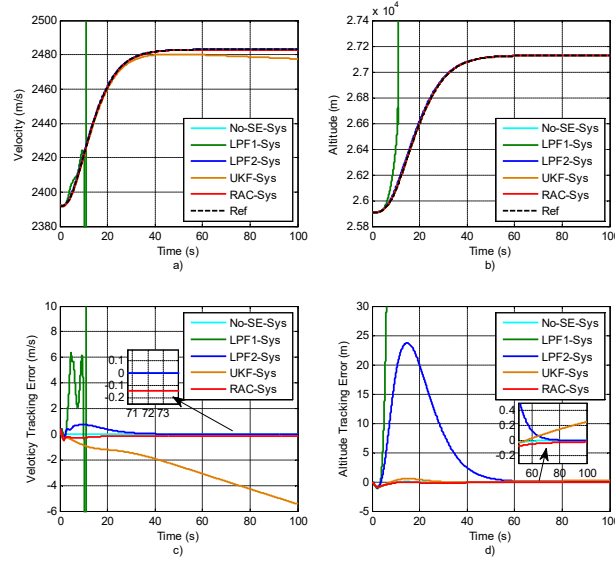


Fig. 5 Responses of a) velocity, b) altitude, c) velocity tracking error and d) altitude tracking error in Scenario 1.

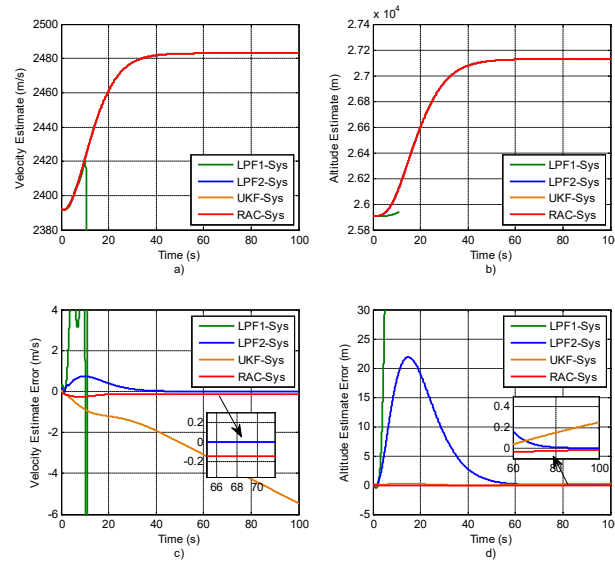


Fig. 6 Results of a) velocity estimate, b) altitude estimate, c) velocity estimate error and d) altitude estimate error in Scenario 1.

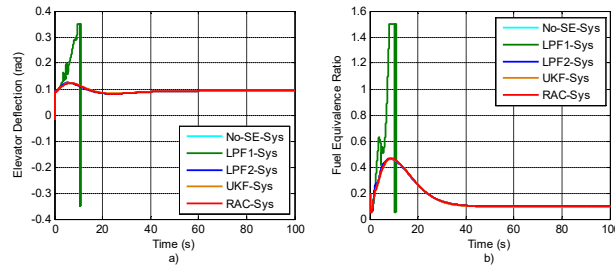


Fig. 7 Control inputs in Scenario 1.

TABLE III
PERFORMANCE CRITERIA IN SCENARIO I

Control System	Velocity Channel			Altitude Channel		
	ISE	IAE	RMSE	ISE	IAE	RMSE
No-SE-Sys	0.1433	0.9197	-	3.7015	9.3589	-
LPF1-Sys	-	-	-	-	-	-
LPF2-Sys	7.1408	13.9584	0.2665	7947.9	482.6429	8.6421
UKF-Sys	931.3804	265.5022	3.0515	6.3943	17.7482	0.1424
RAC-Sys	2.7864	15.9852	0.1549	4.3471	12.8116	0.0389

Scenario 2: In Scenario 2, weak measurement noises are added into the velocity channel and altitude channel, with variances of $0.37 \text{ m}^2/\text{s}^2$ and 9.29 m^2 , respectively, which can be seen in Fig. 8. Since LPF1-Sys has a fail tracking performance in the first scenario, here we only test the performances of No-SE-Sys, LPF2-Sys, UKF-Sys and our proposed RAC-Sys.

The results are given in Fig. 9-11. Although No-SE-Sys has the best tracking performances in the noise-absent scenario, weak measurement noises can bring severe high-frequency chattering of the actuators and make the close-loop system broken down, which indicates a high sensitivity to measurement noises of the FAHV control system. Fig. 10 presents the velocity and altitude estimates. We can see that, compared with measurement noises, unknown flexible dynamics pose more severe side effects on UKF estimate performance, which demonstrates the sensitivity to modeling errors of UKF. In addition, besides the smaller tracking errors in the transition process of our RAC-Sys, it is obvious that under the influence of measurement noises, both the velocity and altitude estimates of RAC-Sys have smaller chattering than those of LPF2-Sys, which demonstrates a stronger filtering property of our proposed state estimator. Fig. 11 shows the control inputs of the four systems. We can see that, both the elevator deflection and the fuel equivalence ratio of our RAC-Sys are smooth and efficacious. As the comparison, although LPF2-Sys can also tackle the tracking problems, there exists small chattering in both control inputs, which will not only cause extra control actions and waste of energy, but also bring vibrations in the FAHV velocity and altitude responses, which can be seen in Fig. 9 c) and d). The performance criteria are shown in TABLE IV, from which we can find that, in this scenario, our RAC-Sys performs the best.

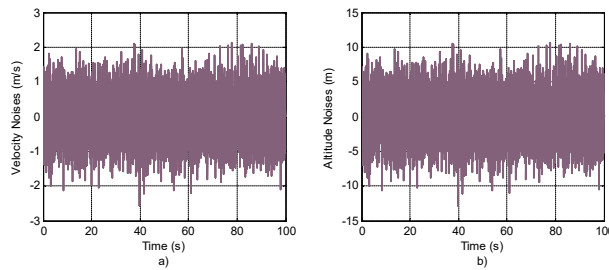


Fig. 8 Measurement noises of a) velocity and b) altitude in Scenario 2.

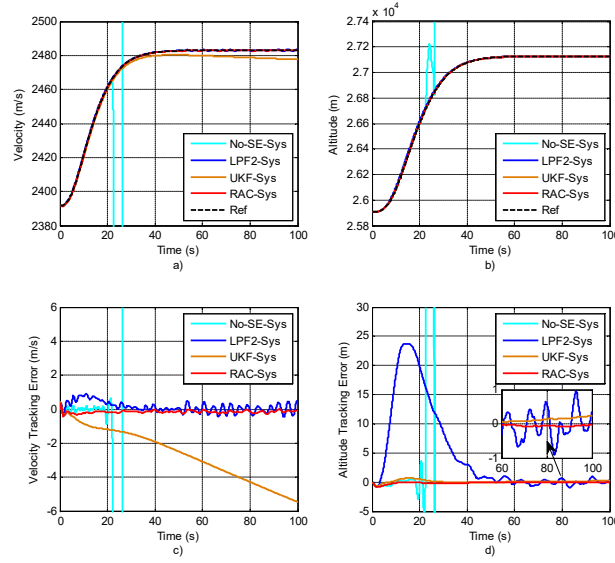


Fig. 9 Responses of a) velocity, b) altitude, c) velocity tracking error and d) altitude tracking error in Scenario 2.

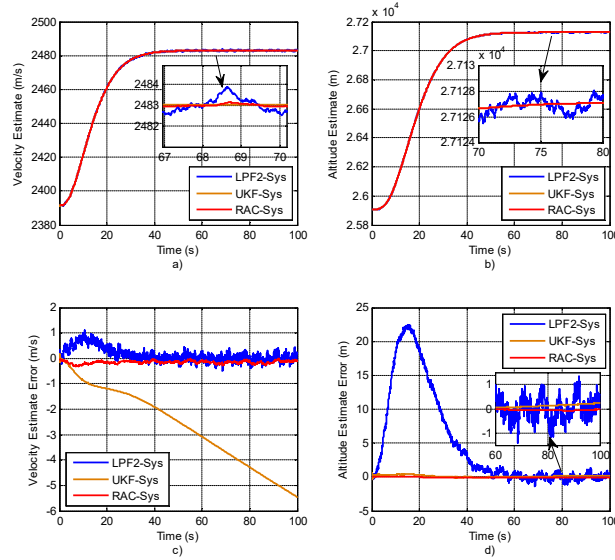


Fig. 10 Results of a) velocity estimate, b) altitude estimate, c) velocity estimate error and d) altitude estimate error in Scenario 2.

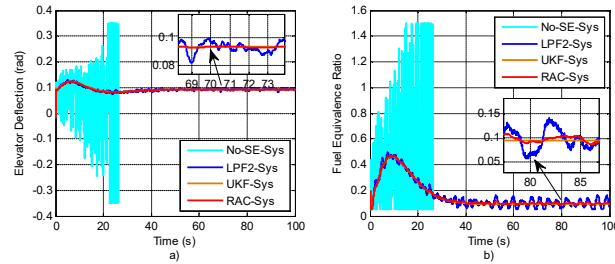


Fig. 11 Control inputs in Scenario 2.

TABLE IV
PERFORMANCE CRITERIA IN SCENARIO 2

Control System	Velocity Channel			Altitude Channel		
	ISE	IAE	RMSE	ISE	IAE	RMSE
No-SE-Sys	-	-	-	-	-	-
LPF2-Sys	10.5863	24.6287	0.2981	7973.1	495.5179	8.6573
UKF-Sys	931.9384	265.0472	3.0525	6.1311	16.8342	0.1780
RAC-Sys	3.1236	16.3133	0.1628	4.2479	13.4896	0.0485

Scenario 3: In this scenario, the velocity and altitude states are contaminated with strong measurement noises, whose variances are $3.34 \text{ m}^2/\text{s}^2$ and 83.61 m^2 , respectively, which can be seen in Fig. 12. Only LPF2-Sys and our proposed RAC-Sys will be evaluated here due to the fail tracking performances of No-SE-Sys and UKF-Sys in Scenario 2, and the results are presented in Fig. 13-15. From Fig. 13, we can see that LPF2-Sys gradually loses control since 35s and totally breaks down at about 62s. Fig. 14 depicts the velocity and altitude estimates. Due to large σ_v and σ_h in LPF2-Sys, the low-pass filtering property of LPF2 is weakened, which results in a huge chattering in those estimates. Fig. 15 shows the control inputs, which demonstrates the failure of the actuators in LPF2-Sys under the effects of strong measurement noises. However, our RAC-Sys can still successfully track the reference signals, with smaller tracking errors, more accurate state estimates as well as smoother control inputs. Thus, it can be concluded that, with such severe measurement noises, our proposed integrated control law can still exhibit a satisfying tracking performance, which verifies the effectiveness and superiority over other comparisons.

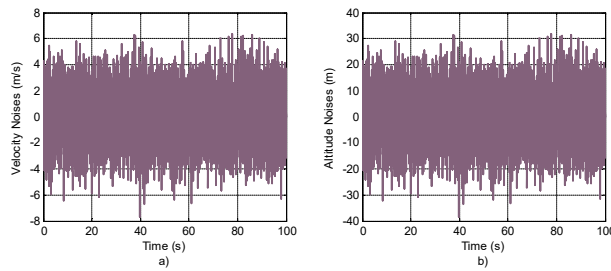


Fig. 12 Measurement noises of a) velocity and b) altitude in Scenario 3.

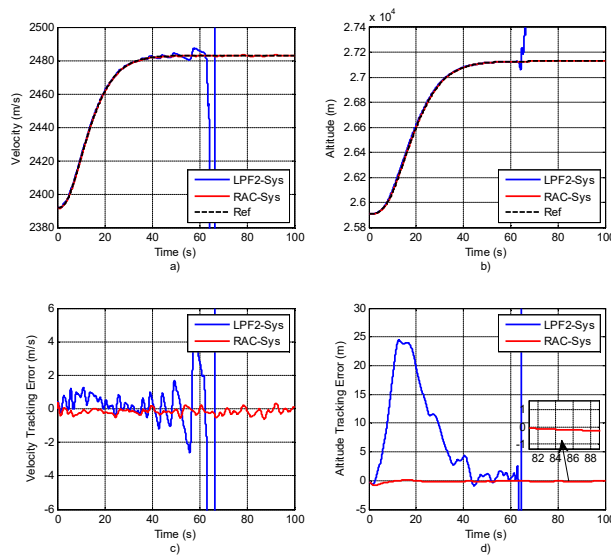


Fig. 13 Responses of a) velocity, b) altitude, c) velocity tracking error and d) altitude tracking error in Scenario 3.

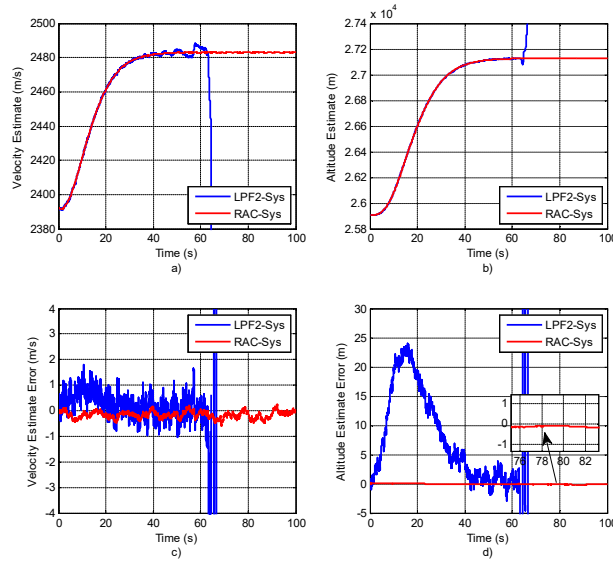


Fig. 14 Results of a) velocity estimate, b) altitude estimate, c) velocity estimate error and d) altitude estimate error in Scenario 3.

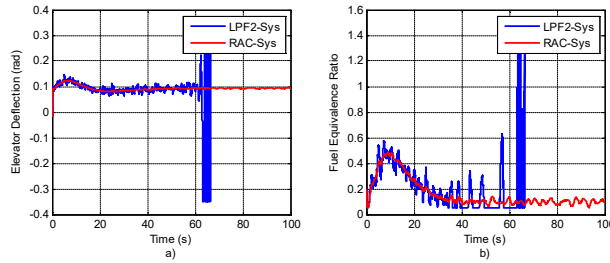


Fig. 15 Control inputs in Scenario 3.

Scenario 4: In the last scenario, a quite intractable case in reality will be simulated, where measurement noises and parametric uncertainties will be simultaneously considered in our proposed integrated control law evaluation. The measurement noises are taken as the same in Scenario 3. Three different levels of constant parametric uncertainties, as 5%, 10% and 15%, are added to the lift L , drag D , thrust T , and pitching moment M_{yy} , where D takes the positive levels while L , T , and M_{yy} take the negative ones.

The simulation results can be seen in Fig. 16-20. From Fig. 16, we can find that, our proposed control law shows a strong robustness against all the three levels of constant parametric uncertainties as well as strong measurement noises and unknown flexible dynamics, despite the fact that with the level of the parametric uncertainties being higher, the tracking errors become a little larger. Compared with the results of the method in [48] shown in Fig. 17, our method can realize smaller tracking errors in both the velocity and altitude tracking, which verifies a stronger robustness property of our proposed control law. The velocity and altitude estimates are given in Fig. 18, which indicates the convergence of our designed state estimator against parametric uncertainties. Fig. 19 depicts the control inputs of the three cases, while the convergence and effectiveness of the IT2-FLSs are demonstrated by Fig. 20. Detail performance criteria can be seen in TABLE V, which intuitively shows the superiority of our proposed method. To sum up, even with severe measurement noises, large parametric uncertainties and unknown flexible dynamics, the proposed control system can still successfully track the given reference signals with satisfying performances, which verifies the robustness of our proposed integrated control law.

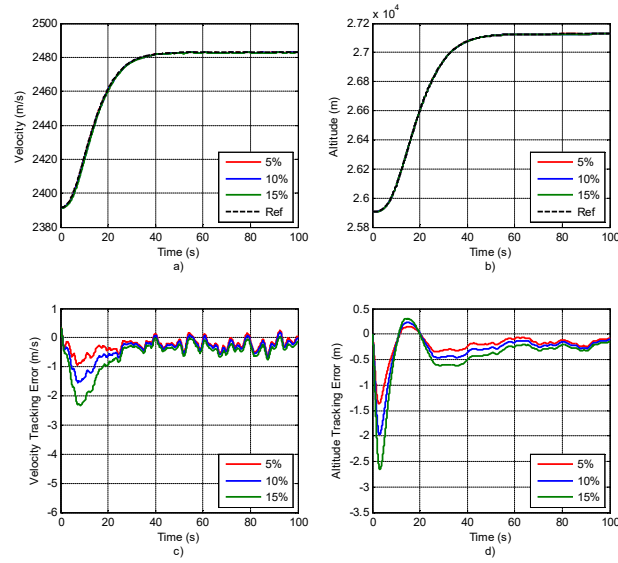


Fig. 16 Responses of a) velocity, b) altitude, c) velocity tracking error and d) altitude tracking error in Scenario 4.

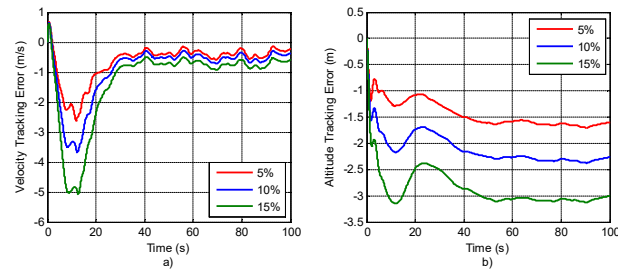


Fig. 17 Responses of a) velocity tracking error and b) altitude tracking error in Scenario 4. (The method in [48])

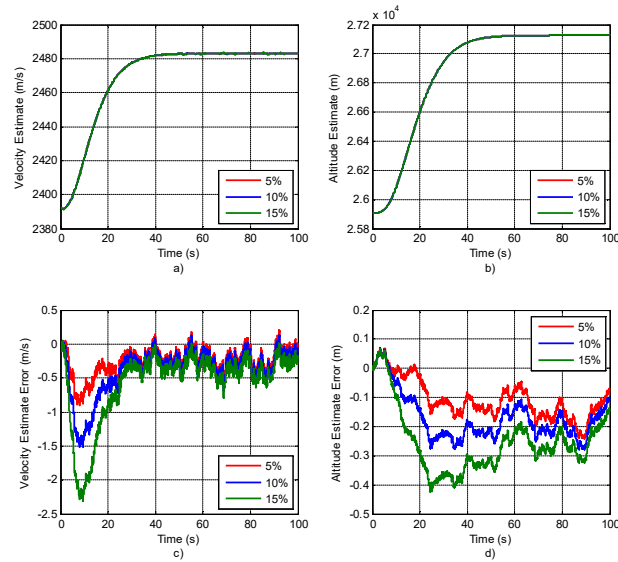


Fig. 18 Results of a) velocity estimate, b) altitude estimate, c) velocity estimate error and d) altitude estimate error in Scenario 4.

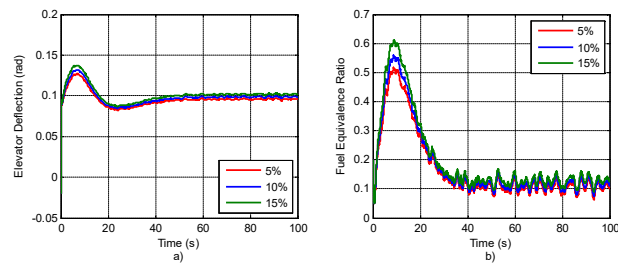


Fig. 19 Control inputs in Scenario 4.

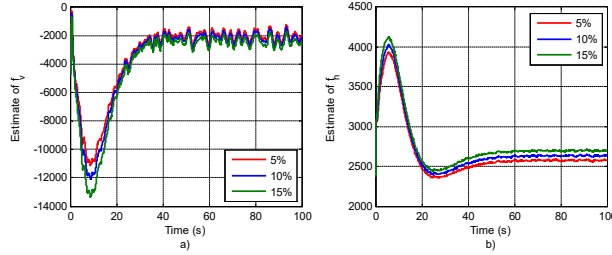


Fig. 20 Outputs of IT2-FLSs in Scenario 4.

TABLE V
PERFORMANCE CRITERIA IN SCENARIO 4

Parametric Uncertainties	Control System	Velocity Channel			Altitude Channel		
		ISE	IAE	RMSE	ISE	IAE	RMSE
5%	RAC-Sys	11.7685	28.4470	0.3202	10.9587	23.5535	0.1257
	Method in [48]	77.5483	65.7819	0.3555	213.3594	143.7989	0.1396
10%	RAC-Sys	27.9356	40.4877	0.5105	22.2492	33.0928	0.1880
	Method in [48]	167.0802	93.4502	0.5535	451.9345	210.4690	0.2067
15%	RAC-Sys	62.5677	58.4932	0.7744	40.4964	44.5555	0.2751
	Method in [48]	338.4849	132.5538	0.8185	833.6954	286.2299	0.2970

V. CONCLUSION

A novel state-estimator-integrated robust adaptive tracking control law is proposed for FAHV to simultaneously deal with measurement noises, parametric uncertainties as well as unknown flexible dynamics in cruise flight stage. The continuous-model-based state estimator is designed to reconstruct the exact states of the velocity and altitude which are contaminated by measurement noises. Based on noise-free measurements, the ideal robust adaptive tracking controller is then constructed, where IT2-FLSs are employed to approximate the unknown dynamics of FAHV online. The stability properties of the state estimator and the ideal state feedback tracking controller are explored through Lyapunov method. Finally, the state-estimator-integrated robust adaptive tracking control law is developed by combining the state estimator and the ideal state feedback tracking controller. Comparative simulations of four scenarios show the robustness and superiority of our proposed integrated control law. Since few investigations of FAHV control design specifically consider the effects of measurement noises on FAHV responses, we believe this study can greatly promote further developments of FAHV applications. In our future work, measurement noises in all the rigid-body states will be considered, and a novel full-order-state-estimator-integrated robust adaptive control system will be investigated.

APPENDIX

The detailed expressions of \mathbf{x} , $\ddot{\mathbf{x}}_0$, ω_1 , Ω_2 , π_1 and Π_2 are given as follows:

$$\mathbf{x} = [V \ \gamma \ \alpha \ \phi \ h]^T, \quad \ddot{\mathbf{x}}_0 = [\ddot{V} \ \ddot{\gamma} \ \ddot{\alpha}_0 \ \ddot{\phi}_0 \ \ddot{h}]^T \text{ where}$$

$$\ddot{\alpha}_0 = \left(z_T T + 0.5 \rho V^2 s \bar{c} \left(C_M^{\alpha^2} \alpha^2 + C_M^\alpha \alpha + C_M^0 \right) \right) / I_{yy} - \ddot{\gamma}$$

$$\ddot{\phi}_0 = -2\zeta_n \omega_n \dot{\phi} - \omega_n^2 \phi$$

$$\omega_1 = \begin{bmatrix} \frac{\partial T}{\partial V} \cos \alpha - \frac{\partial D}{\partial V} \\ -mg \cos \gamma \\ \frac{\partial T}{\partial \alpha} \cos \alpha - T \sin \alpha - \frac{\partial D}{\partial \alpha} \\ \frac{\partial T}{\partial \phi} \cos \alpha \\ -\frac{\partial g}{\partial h} m \sin \gamma \end{bmatrix}^T$$

$$\Omega_2 = [\omega_{21} \ \omega_{22} \ \omega_{23} \ \omega_{24} \ \omega_{25}] \text{ where}$$

$$\omega_{21} = \begin{bmatrix} \frac{\partial^2 T}{\partial V^2} \cos \alpha - \frac{\partial^2 D}{\partial V^2} \\ 0 \\ \frac{\partial^2 T}{\partial \alpha \partial V} \cos \alpha - \frac{\partial T}{\partial V} \sin \alpha - \frac{\partial^2 D}{\partial \alpha \partial V} \\ \frac{\partial^2 T}{\partial \phi \partial V} \cos \alpha \\ 0 \end{bmatrix}, \omega_{22} = \begin{bmatrix} 0 \\ mg \sin \gamma \\ 0 \\ 0 \\ -\frac{\partial g}{\partial h} m \cos \gamma \end{bmatrix}$$

$$\omega_{23} = \begin{bmatrix} \frac{\partial^2 T}{\partial V \partial \alpha} \cos \alpha - \frac{\partial T}{\partial V} \sin \alpha - \frac{\partial^2 D}{\partial V \partial \alpha} \\ 0 \\ \frac{\partial^2 T}{\partial \alpha^2} \cos \alpha - 2 \frac{\partial T}{\partial \alpha} \sin \alpha - T \cos \alpha - \frac{\partial^2 D}{\partial \alpha^2} \\ \frac{\partial^2 T}{\partial \phi \partial \alpha} \cos \alpha - \frac{\partial T}{\partial \phi} \sin \alpha \\ 0 \end{bmatrix}$$

$$\omega_{24} = \begin{bmatrix} \frac{\partial^2 T}{\partial V \partial \phi} \cos \alpha \\ 0 \\ \frac{\partial^2 T}{\partial \alpha \partial \phi} \cos \alpha - \frac{\partial T}{\partial \phi} \sin \alpha \\ \frac{\partial^2 T}{\partial \phi^2} \cos \alpha \\ 0 \end{bmatrix}, \omega_{25} = \begin{bmatrix} 0 \\ -\frac{\partial g}{\partial h} m \cos \gamma \\ 0 \\ 0 \\ -\frac{\partial^2 g}{\partial h^2} m \sin \gamma \end{bmatrix}$$

$$\pi_1 = \left[\begin{array}{c} \frac{\frac{\partial L}{\partial V} + \frac{\partial T}{\partial V} \sin \alpha}{mV} - \frac{L + T \sin \alpha}{mV^2} + \frac{g \cos \gamma}{V^2} \\ \frac{g \sin \gamma}{V} \\ \frac{\frac{\partial L}{\partial \alpha} + \frac{\partial T}{\partial \alpha} \sin \alpha + T \cos \alpha}{mV} \\ \frac{\frac{\partial T}{\partial \phi} \sin \alpha}{mV} \\ \frac{\frac{\partial g}{\partial h} \cos \gamma}{V} \end{array} \right]^T$$

$$\Pi_2 = [\pi_{21} \ \pi_{22} \ \pi_{23} \ \pi_{24} \ \pi_{25}] \text{ where}$$

$$\pi_{21} = \left[\begin{array}{c} \frac{\frac{\partial^2 L}{\partial V^2} + \frac{\partial^2 T}{\partial V^2} \sin \alpha}{mV} - 2 \frac{\frac{\partial L}{\partial V} + \frac{\partial T}{\partial V} \sin \alpha}{mV^2} + 2 \frac{L + T \sin \alpha}{mV^3} - 2 \frac{g \cos \gamma}{V^3} \\ - \frac{g \sin \gamma}{V^2} \\ \frac{\frac{\partial^2 L}{\partial \alpha \partial V} + \frac{\partial^2 T}{\partial \alpha \partial V} \sin \alpha + \frac{\partial T}{\partial V} \cos \alpha}{mV} - \frac{\frac{\partial L}{\partial \alpha} + \frac{\partial T}{\partial \alpha} \sin \alpha + T \cos \alpha}{mV^2} \\ \frac{\frac{\partial^2 T}{\partial \phi \partial V} \sin \alpha}{mV} - \frac{\frac{\partial T}{\partial \phi} \sin \alpha}{mV^2} \\ \frac{\frac{\partial g}{\partial h} \cos \gamma}{V^2} \end{array} \right], \pi_{22} = \left[\begin{array}{c} - \frac{g \sin \gamma}{V^2} \\ \frac{g \cos \gamma}{V} \\ 0 \\ 0 \\ \frac{\frac{\partial g}{\partial h} \sin \gamma}{V} \end{array} \right]$$

$$\pi_{23} = \left[\begin{array}{c} \frac{\frac{\partial^2 L}{\partial V \partial \alpha} + \frac{\partial^2 T}{\partial V \partial \alpha} \sin \alpha + \frac{\partial T}{\partial V} \cos \alpha}{mV} - \frac{\frac{\partial L}{\partial \alpha} + \frac{\partial T}{\partial \alpha} \sin \alpha + T \cos \alpha}{mV^2} \\ 0 \\ \frac{\frac{\partial^2 L}{\partial \alpha^2} + \frac{\partial^2 T}{\partial \alpha^2} \sin \alpha + 2 \frac{\partial T}{\partial \alpha} \cos \alpha - T \sin \alpha}{mV} \\ \frac{\frac{\partial^2 T}{\partial \phi \partial \alpha} \sin \alpha + \frac{\partial T}{\partial \phi} \cos \alpha}{mV} \\ 0 \end{array} \right]$$

$$\pi_{24} = \begin{bmatrix} \frac{\partial^2 T}{\partial V \partial \phi} \sin \alpha & \frac{\partial T}{\partial \phi} \sin \alpha \\ mV & mV^2 \\ 0 & \\ \frac{\partial^2 T}{\partial \alpha \partial \phi} \sin \alpha + \frac{\partial T}{\partial \phi} \cos \alpha & \\ mV & \\ \frac{\partial^2 T}{\partial \phi^2} \sin \alpha & \\ mV & \\ 0 & \end{bmatrix}, \pi_{25} = \begin{bmatrix} \frac{\partial g}{\partial h} \cos \gamma \\ V^2 \\ \frac{\partial g}{\partial h} \sin \gamma \\ V \\ 0 \\ 0 \\ \frac{\partial^2 g}{\partial h^2} \cos \gamma \\ V \end{bmatrix}$$

REFERENCES

- [1] B. Xu and Z. Shi, "An overview on flight dynamics and control approaches for hypersonic vehicles," *Sci. CHINA Inf. Sci.*, vol. 58, no. 7, pp. 1–19, Jul. 2015.
- [2] J. A. Echols, K. Puttannaiah, K. Mondal, and A. Rodriguez, "Fundamental control system design issues for scramjet-powered hypersonic vehicles," in *AIAA Guid., Navig., Control Conf.*, Kissimmee, Florida, USA, 2015.
- [3] Z. Pu, X. Tan, G. Fan, and J. Yi, "Uncertainty analysis and robust trajectory linearization control of a flexible air-breathing hypersonic vehicle," *Acta Astronaut.*, vol. 101, no. 1, pp. 16–32, Aug.–Sep. 2014.
- [4] D. O. Sighthorsson, P. Jankovsky, A. Serrani, S. Yurkovich, M. A. Bolender, and D. B. Doman, "Robust linear output feedback control of an airbreathing hypersonic vehicle," *J. Guid. Control Dyn.*, vol. 31, no. 4, pp. 1052–1066, Jul.–Aug. 2008.
- [5] M. A. Bolender and D. B. Doman, "Nonlinear longitudinal dynamical model of an air-breathing hypersonic vehicle," *J. Spacecr. Rockets*, vol. 44, no. 2, pp. 374–387, Mar.–Apr. 2007.
- [6] T. E. Gibson, L. G. Crespo, and A. M. Annaswamy, "Adaptive control of hypersonic vehicles in the presence of modelling uncertainties," in *Proc. Amer. Control Conf.*, St. Louis, MO, USA, 2009, pp. 3178–3183.
- [7] X. Hu, L. Wu, C. Hu, and H. Gao, "Adaptive sliding mode tracking control for a flexible air-breathing hypersonic vehicle," *J. Frankl. Inst.*, vol. 349, no. 2, pp. 559–577, Mar. 2012.
- [8] J. Wang, Q. Zong, R. Su, and B. Tian, "Continuous high order sliding mode controller design for a flexible air-breathing hypersonic vehicle," *ISA Trans.*, vol. 53, no. 3, pp. 690–698, May 2014.
- [9] Q. Zong, J. Wang, B. Tian, and Y. Tao, "Quasi-continuous high-order sliding mode controller and observer design for flexible hypersonic vehicle," *Aerosp. Sci. Technol.*, vol. 27, no. 1, pp. 127–137, Jun. 2013.
- [10] L. Fiorentini, A. Serrani, M. A. Bolender, and D. B. Doman, "Nonlinear robust adaptive control of flexible air-breathing hypersonic vehicles," *J. Guid. Control Dyn.*, vol. 32, no. 2, pp. 401–416, Mar. 2009.
- [11] X. Su and Y. Jia, "Constrained adaptive tracking and command shaped vibration control of flexible hypersonic vehicles," *IET Control Theory Appl.*, vol. 9, no. 12, pp. 1857–1868, Aug. 2015.
- [12] J. He, R. Qi, B. Jiang, and J. Qian, "Adaptive output feedback fault-tolerant control design for hypersonic flight vehicles," *J. Franklin Inst.*, vol. 352, no. 5, pp. 1181–1835, May 2015.
- [13] L. Dou, P. Su, and Z. Ding, "Modeling and nonlinear control for air-breathing hypersonic vehicle with variable geometry inlet," *Aerosp. Sci. Technol.*, vol. 67, pp. 422–432, Aug. 2017.
- [14] J. Gao, R. Yuan, J. Yi, and C. Li, "Indirect adaptive interval type-2 fuzzy sliding mode controller design for flexible air-breathing hypersonic vehicles," *IFAC-PapersOnLine*, vol. 50, no. 1, pp. 3007–3013, Jul. 2017.
- [15] X. Hu, L. Wu, C. Hu, and H. Gao, "Fuzzy guaranteed cost tracking control for a flexible air-breathing hypersonic vehicle," *IET Control Theory Appl.*, vol. 6, no. 9, pp. 1238–1249, Jun. 2012.
- [16] B. Xu, D. Wang, Y. Zhang, and Z. Shi, "DOB-Based neural control of flexible hypersonic flight vehicle considering wind effects," *IEEE Trans. Ind. Electron.*, vol. 64, no. 11, pp. 8676–8685, Nov. 2017.
- [17] X. Bu, X. Wu, D. Wei, and J. Huang, "Neural-approximation-based robust adaptive control of flexible air-breathing hypersonic vehicles with parametric uncertainties and control input constraints," *Inf. Sci.*, vol. 346–347, pp. 29–43, Jun. 2016.
- [18] X. Bu, X. Wu, J. Huang, Z. Ma, and R. Zhang, "Minimal-learning-parameter based simplified adaptive neural back-stepping control of flexible air-breathing hypersonic vehicles without virtual controllers," *Neurocomputing*, vol. 175, pp. 816–825, Jan 2016.

- [19] X. Bu, G. He, and K. Wang, "Tracking control of air-breathing hypersonic vehicles with non-affine dynamics via improved neural back-stepping design," *ISA Trans.*, vol. 75, pp. 88–100, Apr. 2018.
- [20] L. Ye, Q. Zong, J. L. Crassidis, and B. Tian, "Output-redefinition-based dynamic inversion control for a nonminimum phase hypersonic vehicle," *IEEE Trans. Ind. Electron.*, vol. 65, no. 4, pp. 3447–3457, Apr. 2018.
- [21] X. Hu, B. Xu, and C. Hu, "Robust adaptive fuzzy control for HFV with parameter uncertainty and unmodeled dynamics," *IEEE Tran. Ind. Electron.*, vol. 65, no. 11, pp. 8851–8860, Nov. 2018.
- [22] X. Bu, "Guaranteeing prescribed performance for air-breathing hypersonic vehicles via an adaptive non-affine tracking controller," *Acta Astronaut.*, vol. 151, pp. 368–379, Oct. 2018.
- [23] Y. Liu, Z. Pu, and J. Yi, "Observer-based robust adaptive T2 fuzzy tracking control for flexible air-breathing hypersonic vehicles," *IET Control Theory Appl.*, vol. 12, no. 8, pp. 1036–1045, May 2018.
- [24] Q. Zong, Y. Ji, F. Zeng, and H. Liu, "Output feedback back-stepping control for a generic hypersonic vehicle via small-gain theorem," *Aerosp. Sci. Technol.*, vol. 23, no. 1, pp. 409–417, Dec. 2012.
- [25] X. Bu, X. Wu, Z. Ma, and R. Zhang, "Nonsingular direct neural control of air-breathing hypersonic vehicle via back-stepping," *Neurocomputing*, vol. 153, pp. 164–173, Apr. 2015.
- [26] Z. Liu, X. Tan, R. Yuan, G. Fan, and J. Yi, "Immersion and invariance-based output feedback control of air-breathing hypersonic vehicles," *IEEE Trans. Autom. Sci. Eng.*, vol. 13, no. 1, pp. 394–402, Jan. 2016.
- [27] X. Bu, X. Wu, R. Zhang, Z. Ma, and J. Huang, "Tracking differentiator design for the robust backstepping control of a flexible air-breathing hypersonic vehicle," *J. Franklin Inst.*, vol. 352, no. 4, pp. 1739–1765, Apr. 2015.
- [28] S. A. Whitmore and T. R. Moes, "Measurement uncertainties and feasibility study of a flush airdata system for a hypersonic flight experiment," *NASA Technical Memorandum 4627*, 1994.
- [29] P. Motyka, W. Bonnice, S. Hall, and E. Wagner, "The evaluation of failure detection and isolation algorithms for reconstructurable control," *NASA Contractor Report 177983*, 1985.
- [30] M. R. Napolitano, Y. An, and B. A. Seanor, "A fault tolerant flight control system for sensor and actuator failures using neural networks," *Aircraft Des.*, vol. 3, no. 2, pp. 103–128, Jun. 2000.
- [31] C. Han, Z. Liu, and J. Yi, "Immersion and invariance adaptive control with σ -modification for uncertain nonlinear systems," *J. Franklin Inst.*, vol. 355, no. 5, pp. 2091–2111, Mar. 2018.
- [32] J. Yao, Z. Jiao, D. Ma, and L. Yan, "High-accuracy tracking control of hydraulic rotary actuators with modeling uncertainties," *IEEE ASME Trans. Mechatron.*, vol. 19, no. 2, pp. 633–641, Apr. 2014.
- [33] J. Yao, W. Deng, and Z. Jiao, "RISE-based adaptive control of hydraulic systems with asymptotic tracking," *IEEE Trans. Autom. Sci. Eng.*, vol. 14, no. 3, pp. 1524–1531, Jul. 2017.
- [34] X. Tao, J. Yi, G. Fan, and J. Zhang, "Adaptive non-singleton interval type-2 fuzzy logic controller design for flexible air-breathing hypersonic vehicles against measurement noises," in *the 7th Int. Symp. Comput. Intell. Ind. Appl. (ISCIIA 2016)*, Beijing, China, 2016.
- [35] K. Reif and R. Unbehauen, "The extended kalman filter as an exponential observer for nonlinear systems," *IEEE Trans. Signal Process.*, vol. 47, no. 8, pp. 2324–2328, Aug. 1999.
- [36] Y. Wu, D. Hu, M. Wu, and X. Hu, "Unscented kalman filtering for additive noise case: augmented versus nonaugmented," *IEEE Signal Process. Lett.*, vol. 12, no. 5, pp. 357–360, May 2005.
- [37] M. Partovibakhsh and G. Liu, "An adaptive unscented kalman filtering approach for online estimation of model parameters and state-of-charge of lithium-ion batteries for autonomous mobile robots," *IEEE Trans. Control Syst. Technol.*, vol. 23, no. 1, pp. 357–363, Jan. 2015.
- [38] K. A. Kramer, S. C. Stubberud, and J. A. Geremia, "Target registration correction using the neural extended kalman filter," *IEEE Trans. Instrum. Meas.*, vol. 59, no. 7, pp. 1964–1971, Jul. 2010.
- [39] M. Saha, R. Ghosh, and B. Goswami, "Robustness and sensitivity metrics for tuning the extended kalman filter," *IEEE Trans. Instrum. Meas.*, vol. 63, no. 4, pp. 964–971, Apr. 2014.
- [40] N. Enayati, E. D. Momi, and G. Ferrigno, "A Quaternion-based unscented kalman filter for robust optical/inertial motion tracking in computer-assisted surgery," *IEEE Trans. Instrum. Meas.*, vol. 64, no. 8, pp. 2291–2301, Aug. 2015.
- [41] R. G. Valenti, I. Dryanovski, and J. Xiao, "A linear kalman filter for MARG orientation estimation using the algebraic quaternion algorithm," *IEEE Trans. Instrum. Meas.*, vol. 65, no. 2, pp. 467–481, Feb. 2016.
- [42] A. Sharma, S. C. Srivastava, and S. Chakrabarti, "A cubature kalman filter based power system dynamic state estimator," *IEEE Trans. Instrum. Meas.*, vol. 66, no. 8, pp. 2036–2045, Aug. 2017.
- [43] N. Sadegh and R. Horowitz, "Stability and robustness analysis of a class of adaptive controllers for robot manipulators," *Int. J. Rob. Res.*, vol. 9, no. 3, pp. 74–92, Jun. 1990.

- [44] J. Yao, W. Deng, and W. Sun, "Precision motion control for electro-hydraulic servo systems with noise alleviation: a desired compensation adaptive approach," *IEEE ASME Tran. Mechatron.*, vol. 22, no. 4, pp. 1859–1868, Aug. 2017.
- [45] Y. Hong and B. Yao, "A globally stable saturated desired compensation adaptive robust control for linear motor systems with comparative experiments," *Automatica*, vol. 43, no. 10, pp. 1840–1848, Oct. 2007.
- [46] Z. Peng, D. Wang, W. Wang, and L. Liu, "Neural adaptive steering of an unmanned surface vehicle with measurement noises," *Neurocomputing*, vol. 186, no. 19, pp. 228–234, Apr. 2016.
- [47] D. Astolfi, L. Marconi, L. Praly, and A. Teel, "Sensitivity to high-frequency measurement noise of nonlinear high-gain observers," *IFAC-PapersOnLine*, vol. 49, no. 18, pp. 862–866, 2016.
- [48] X. Tao, J. Yi, R. Yuan, and Z. Liu, "Control of a flexible air-breathing hypersonic vehicle with measurement noises using adaptive interval type-2 fuzzy logic system," in *IEEE Int. Conf. Fuzzy Syst.*, Naples, Italy, 2017.
- [49] J. T. Parker, A. Serrani, S. Yurkovich, M. A. Bolender, and D. B. Doman, "Control-oriented modeling of an air-breathing hypersonic vehicle," *J. Guid. Control Dyn.*, vol. 30, no. 3, pp. 856–869, May–Jun. 2007.
- [50] L. Fiorentini, "Nonlinear adaptive controller design for air-breathing hypersonic vehicles," Ph. D dissertation, Electrical and Computer Engineering Department, The Ohio State University, 2010.
- [51] J. M. Mendel, R. I. John, and F. Liu, "Interval type-2 fuzzy logic systems made simple," *IEEE Trans. Fuzzy Syst.*, vol. 14, no. 6, pp. 808–821, Dec. 2006.
- [52] H. Ying, "General interval type-2 Mamdani fuzzy systems are universal approximators," in *Annu. Conf. North Am. Fuzzy Inf. Process. Soc.*, New York, USA, 2008.
- [53] H. Xu, M. D. Mirmirani, and P. A. Ioannou, "Adaptive sliding mode control design for a hypersonic flight vehicle," *J. Guid. Control Dyn.*, vol. 27, no. 5, pp. 829–838, Sep.–Oct. 2004.
- [54] Q. Wang and R. F. Stengel, "Robust nonlinear control of a hypersonic aircraft," *J. Guid. Control Dyn.*, vol. 23, no. 4, pp. 577–585, Jul.–Aug. 2000.
- [55] J. M. Mendel, "On KM algorithms for solving type-2 fuzzy set problems," *IEEE Trans. Fuzzy Syst.*, vol. 21, no. 3, pp. 426–446, Jun. 2013.
- [56] J. H. Ahrens and H. K. Khalil, "High-gain observers in the presence of measurement noise: a switched-gain approach," *Automatica*, vol. 45, no. 4, pp. 936–943, Apr. 2009.
- [57] M. A. Bolender and D. B. Doman, "Flight path angle dynamics of air-breathing hypersonic vehicles," in *AIAA Guid. Navig. Control Conf. 2006*, Keystone, CO, USA, 2006, pp. 4637–4661.